Astrophysics with Intense and Ultra-Intense Lasers "Laser Astrophysics"

Hideaki TAKABE*)

Institute of Laser Energetics and Graduate School of Science
Osaka University, Suita 565-0871, Japan

(Received July 12, 2001)

I review the present status of laser astrophysics research in which the intense and ultra-intense lasers are used to study basic data of hot-dense plasmas, violent phenomena such as explosion scaled down in laboratory with appropriate similarity law, and advanced physics such as anti-matter plasmas. The author's original discipline, laser fusion, requires studying the physics of high-energy density (HED) plasmas. Modern astrophysics also needs the maturity of HED physics. I briefly review the physics scenario of laser fusion and divide it to six subjects. They are (1) Laser plasma interaction, (2) Electron energy transport, (3) Hydrodynamics and strong shocks, (4) Hydrodynamic instability, (5) Atomic physics and X-ray transport, and (6) Laser-produced relativistic plasmas. The author proposed to introduce three views to consider and pick up model experiments suggested from each topics in laser fusion. They are (1) Sameness, (2) Similarity, and (3) Resemblance. The matrix made of six rows of the subjects of laser fusion and three columns of three views gave us at the present time fifteen subjects of laser astrophysics. These fifteen topics include, for example, the equation of state and opacity of the hot-dense plasmas, topics related to supernova explosions, and relativistic electron-positron plasma jets seen in active galactic nuclei. The detailed explanation on astrophysical interest and possible model experiments for each topics is given in the present paper. I hope that this paper will motivate the readers to think and find a variety of new topics and the matrix table becomes black with many new key words.

Contents

*) E-mail: takabe@ile.osaka-u.ac.jp

§1. Introduction

The universe cannot be claimed as the sole domain of any one particular field of scientific study. It is, however, the most studied and longest studied subject of science. Starting in ancient times, mankind has sought to understand the behavior of the stars, and thereby glean the "will of the heavens". With the invention of the first simple telescopes, however, mankind was confronted for the first time with quantitative data on the motions of the planets. The data were in clear disagreement with the planetary theories of that era, leading to a complete reformulation of the theory of the solar system. This heralded the dawning of modern astronomy. And so the cycle continues today, with ever more precise instruments taking ever more far-reaching data, stretching our minds and imaginations to ponder the beginnings and endings of stars, galaxies, and even the universe as a whole.

The methods for studying "the heavens" have advanced greatly with time. Recently, the universe has been mapped out in detail, owing to the development of the CCD camera and advanced telescopes, both on land and in satellites. With these quantum leaps in technology, the quality of quantitative astronomical data has improved dramatically. As a result, it is no longer sufficient to explain these high quality quantitative data with broad, qualitative explanations. Astrophysicists are now resorting to large scale numerical simulations with sophisticated computer codes to attempt to quantitatively explain everything from the large scale structure of universe to the birth and death of stars.

On a separate front, research in the field of laser fusion has reached a level of considerable maturity, with investigations conducted both of fundamental physics processes and of integral experiments such as capsule implosions. Compressible fluid dynamics, radiation hydrodynamics, and atomic physics are all required to do quantitative analyses of the laser fusion experiments. These same physics processes are also required in astrophysics research. Clearly, both astrophysics and laser fusion stand to benefit by using high-intensity lasers for detailed study of plasmas in extreme conditions.

The astrophysics aims at clarifying the evolution scenario from the Big Bang to the present structure of the universe. Therefore, if ambiguities in the physical processes in constructing the theories of galaxy formation, star formation, increase of heavy elements due to nuclear synthesis in supernovae, and so on can be clearer with model experiments, the entitled research will grow as a new research field for the fundamental physics. It is meaningless just to say that the laser-produced plasmas resemble those observed in the universe. We have to look for a research scenario with which a part of the critical issues for astrophysics can be solved with lasers.

When intense or ultra-intense lasers are irradiated on matters, high-density and high-temperature plasmas are produced. The physics of such plasmas which is called HED (high energy density) physics,[1)] has the same base as the core physics of astrophysics. It was pointed out from the beginning of laser plasma research that the astrophysics is an important subject for laser plasma.[2)] After 40 years from the beginning, the laser technology and laser plasma physics have come to the stage of maturity and the possibility of "laser astrophysics" has become realistic. It is beneficial for both scientists in fusion and astrophysics to study HED physics by modeling astrophysical phenomena with intense and ultra-intense lasers.

We can roughly divide the elements of astrophysics after the three minutes from the Big Bang into the following five:

(I) Hydrodynamics and magneto-hydrodynamics,
(II) Atomic physics, radiation transport and radiation hydrodynamics,
(III) Relativistic plasmas,
(IV) Nuclear reactions,
(V) Gravitational interactions.

It is difficult to do some model experiments of the item (V) in the laboratory, while a variety of model experiments can be designed concerning the items (I)–(III) by use of intense and ultra-intense lasers. The ultra-intense lasers may be used to generate relativistic electron-positron plasmas. The item (IV) is principally possible to be studied with laser-produced fusion plasmas. For studying the detail of this physics, however, an extremely high temperature only achieved by thermonuclear reaction in an imploded fusion fuel is required. In this case, a big laser facility of multi-beam system such as National Ignition Facility (NIF)[3)] or Laser-Mega-Joule (LMJ)[4)] would be necessary. For studying magneto-hydrodynamics (MHD) phenomena such as collision-less shocks of Supernova remnants (SNRs) and magnetic reconnection phenomena observed in the solar flare, it is necessary to produce the plasma in external magnetic fields or laser-generated magnetic field.

On the basis of the similarity transformation, the important physics such as hydrodynamic instabilities of supernova explosion and interaction between high Mach number shock wave and ISM (interstellar media) can be modeled in the laboratory to clarify controlling physics.[5)]

A model experiment for a strong blast wave has been carried out by Ripin et al.[6)] relating to SNRs and an instability of the blast wave front due to radiation cooling which is now called "Vishinac instability" has been observed.[7)] The similarity and difference of the hydrodynamic instability in the supernova 1987A (SN1987A) was discussed by the author comparing it with that in laser-driven implosion.[5)] Model

experiments have been carried out in US regarding highly nonlinear stage of the R-T instability in supernova explosion.[8] These are summarized in a series of review papers written as a joint work with the author.[9-11]

Line X-rays and γ-rays are good objects for new astrophysics research. For example, observational data with X-ray satellite "ASCA" are used to estimate the abundance in SNRs.[12] The line X-rays are emitted from SNRs, which is still in the ionizing phase even after 10^3 years from a supernova (SN) explosion. In order to calculate the material abundance of Si, Mg, and so on from the data, a rate equation solver to evaluate non-local thermodynamic equilibrium (non-LTE) atomic state is necessary. Such numerical solver has to be checked by comparing it with well-defined experiments, and the laser-produced plasma can be a good candidate for this purpose. In this case, the temperature is almost same as SNR plasma, while the density and the time scale are very different. However, we can design a reasonable model experiment by adjusting the ionization parameter defined by the product of the density and time as will be discussed later. In addition, spectral opacity of relatively heavy elements with density and temperature near stellar surface or interior has been studied with the name of "opacity experiment" with a combination of laser heating and X-ray back-lighting by use of laser produced radiation.

The opening new field called "laser astrophysics" is based on a big progress of laser technology. During 40 years from the invention of laser, the power of intense lasers has progressed dramatically from kW to PW (peta-watt). The diagram of annual growth of the maximum available laser power is plotted on the right in Fig. 1. This figure indicates that the power increased by factor ten every three years in average as estimated from the dotted line. In the field of accelerator, the left figure of Fig. 1 is called "Livingstone Chart".[13] As is clear from this figure, the beam energy of accelerators has increased for the last 60 years by a factor 10 every six years. It is clear that the high power laser has grown as a new tool to investigate an advanced physics in extreme conditions. This rapid growth of the laser technology is partially driven by the need for laser fusion research and also by the invention of CPA (Chirped Pulse Amplification) technology.[14] I have strong confidence that such dramatic progress of laser technology opens a new field of science called "Intense Laser Science".

The physics scenario of laser fusion is summarized in Appendix A. In what follows, we use the word inertial confinement fusion (ICF) as almost the same meaning as laser fusion. From the laser irradiation on a spherical target to the final fusion burn, we can roughly divide the physics issues to six. They are:

(1) Laser-plasma interactions,
(2) Electron energy transports,
(3) Hydrodynamics and strong shocks,
(4) Hydrodynamic instabilities,
(5) Atomic physics and X-ray radiation transports,
(6) Laser produced relativistic plasmas.

When an intense laser is irradiated on a target, the physics of the item (1) should be studied. By laser-plasma interaction, most of laser energy is used to heat electrons and kinetics of electron energy transport becomes important. The electron energy is

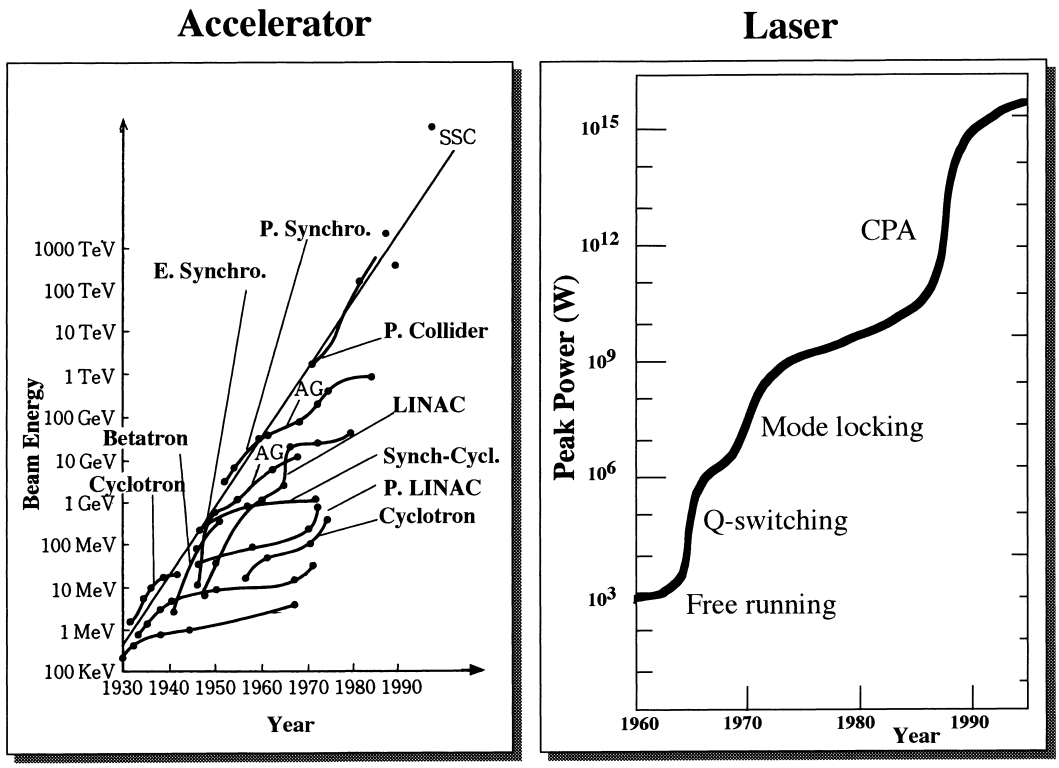

Fig. 1. Historical evolution of the beam energy of the accelerator (left) and that of the peak power of the intense laser (right). The left figure is called "Livingston chart" and the right figure can be called the Livingstone chart of intense laser. It should be noted that the beam energy of the accelerator has progressed ten times every six years in the last 70 years, while the peak power of laser has increased ten times every three years on average.

carried to the over-dense region and generates extremely high pressure over the surface of the target. Then, strong shock waves are generated and compressible hydrodynamics should be studied. Since the target shell is accelerated toward the center by the high-temperature but relatively low-density ablating plasma, the ablation front becomes unstable to Rayleigh-Taylor instability. In addition, Richtmyer-Meshkov instability driven by shock wave also appears to be important in the implosion process. In order to control the density profile so as to reduce the growth of such instabilities, medium-Z material is doped in the target. Then, the X-ray transport becomes important issue to be studied. In addition, soft X-ray efficiently generated with intense laser irradiation on high-Z solid is also important in X-ray driven implosion.[15] The high-Z atom is in general not in local thermodynamic equilibrium. Therefore, complicated atomic physics and atomic process should be studied. Recently, the technical accomplishment of PW laser made the fast-ignition laser-fusion scheme[16] possible. In this fusion scheme, an ultra-intense laser is impinged at the edge of the compressed core. Then, the electric field of the focused beam becomes 10 keV/Å and high energy electrons generated have energy in the range of 10 MeV. The relativistic plasma physics became one of the important issues to be studied in

laser fusion recently.

On the other hand, there are three views which relate the laser-produced plasmas to astrophysics. They are:

(a) Sameness of physics,
(b) Similarity of physical dynamics,
(c) Resemblance of physics.

At first, it is easy to understand the meaning of the term (a). This means to produce plasma with the same temperature and density as the surface or interior of stars and to study, for example, the equation of state (EOS) and the emissivity and opacity of X-rays. In addition, if we are able to use a huge laser system like NIF (National Ignition Facility), we may also be able to study the cross sections and their density dependence of thermonuclear fusion reactions important inside stars.

The term (b) represents the study of physical evolution in time and space of compressible hydrodynamics, atomic processes, etc. For example, we reproduce the physics of supernova remnants with the diameter of a few tens ly (light year) and the age of a few thousand years by reducing the scale of time and space by a factor 10^{20} in the blast wave driven by laser light. This concept is same as the design of aircraft by putting a small-scale model in a wind tunnel. In this case, the non-dimensional parameters, Reynolds number and Mach number, should be kept same as those for a real aircraft in flight. In the case of the wind tunnel, the scaling factor is about 10^3. The difference from the case of the wind tunnel is extremely large difference of the scaling factor. Another examples of the term (b) are very strong shock and matter interactions, hydrodynamic instabilities of the case where energy transports essentially modify the growth of the instabilities, non-local thermodynamic equilibrium phenomena, radiation hydrodynamic phenomena and so on.

The term (c) represents the case where although scaling law is not found yet, physics and phenomena very resemble each other. For example, it indicates the creation of anti-matter by use of ultra-intense lasers and electron-positron plasma formation. There are full of electron-positron plasmas near Black Hole and also in AGNs (Active Galactic Nuclei). We plan to do an experiment where the generated electron-positron plasma collides with imposed magnetic field or matter. Such experiment may be a model experiment of expanding fire-ball believed to be important as the energy source of the γ-ray bursts. At the same time, it is also interesting to study photo-nuclear reaction processes. The demonstration of possibility of X-ray laser astro-objects is also included in the term (c). It is reported that photo-ionized plasma is observed near the X-ray compact object, Cygnus X-3. The plasma with temperature roughly equal to 10–20 eV is under strong irradiation of hard X-ray coming from a companion black hole or neutron star. This low temperature plasma is photo-ionized to emit many strong line emission from metal such as Si, Mg. By irradiating lasers in a gold cavity we can generate almost Planckian X-ray source with temperature up to about 300 eV.[15] By providing a low temperature plasma at the same time, we can observe the atomic state distribution of photo-ionized plasma under the irradiation of this X-ray source. Systematic study of the photo-ionized plasma will lead us to clarifying the condition for photo-pumping X-ray lasing in the universe.

Table I. The matrix to consider and find model experiments of laser astrophysics. The six rows indicate the main subjects to study laser fusion, while the three columns are three views to replace the subjects of laser fusion to the topics of laser astrophysics. At the present time, the author could enumerate 15 topics in this matrix, the details of most of which are describe in the present paper according this order.

	1. Sameness	2. Similarity	3. Resemblance
1. Laser-Plasma Interaction			
2. Electron Energy Transport			
3. Hydrodynamics and Shocks	1. Equation of State (Giant Planets)	2. Interaction of Molecular Cloud with Strong Shock by SNR (Morphology)	3. Collision-less Shocks and Particle Acceleration (Origin of Cosmic Ray)
4. Hydrodynamic Instability		4. RT Instability of SN Explosion (SN1987A)	5. Hydro-Instability in Neutrino-Driven SN Explosion 6. RT Instability of Eagle Nebula
5. Atomic Physics and X-ray Transport	7. Opacity (Star Evolution, etc.)	8. Non-LTE Atomic Process in SNR 9. Stellar Jets (Non-Rel.) 10. Radiation Hydro. (Early Galaxy) 11. Photo-ionized Plasmas	12. Vishiniac Instability of SNR 13. X-ray Laser in Universe
6. Laser-Produced Relativistic Plasma			14. Fireball of Gamma-ray Bursts 15. Cosmological Jets (Rel.)

Closing this session, I would like to show the crossover of the subjects targeted in the laser astrophysics in Table I. In Table I, the vertical axis having six frames means the subject important in laser fusion research as explained in Appendix A. In contrast, the horizontal axis has three frames as mentioned already. We can consider a variety of model experiments at the crossing frame of both axes. At the present time, I cannot find any good example regarding the two subjects, laser plasma interactions, and electron kinetic energy transport some details of which are explained in Appendix B. The latter is rather fundamental issues and the numerical methods or theoretical modeling will be used to the transport of neutrino, etc., for example, in supernova explosion modeling. There are many subjects found rather easily regarding the other four topics. At the present time, fifteen subjects can be enumerated in my mind; some of them have already been studied experimentally. In the present paper, I would like to describe more details concerning these subjects.

In §2, the properties of laser produced plasma are explained and diagnostics of laser plasmas are briefly reviewed. From §3 to §6, we explain more details of the subjects listed in Table I. In §3, the subjects relating to hydrodynamics and strong shocks are described. In §4, the topics relating to hydrodynamic instability are explained. In §5, the topics relating to atomic physics and X-ray transport are described. Section 6 is devoted to the topics of relativistic plasmas, especially, positron formation and electron-positron plasmas. In §7, we briefly discuss the possibility to apply the

laser foil acceleration to study the properties of optical signal coming from the falling material into a black hole. In this case, the discussing point is the applicability of Einstein's "equivalence principle" between the extremely strong gravitational force near the black hole and the extremely strong acceleration of the foil by intense short pulse lasers. In this section a brief summary and future prospect are also given.

§2. What is the laser plasma?

When an intense laser is irradiated on a solid material as shown in Fig. 2(a), the laser energy is absorbed at very beginning by the multi-photon absorption process and free electrons are produced. If the free electrons have enough kinetic energies, they enhance the ionization of the material through the collisional ionization process. Once the partially ionized plasma is produced, the free electrons predominantly contribute to the absorption of the still-coming laser energy. This absorption process is called "inverse-bremsstrahlung" absorption. This is the inverse process of radiation emission stemming from the collision between an electron and an ion. The free electrons obtain the energy of laser photons in colliding with ions. The free electrons quiver in the electric field of laser light, and their motion is almost harmonic oscillation in the plane of the electric field. If we can neglect the collional process, the motion is reversible. When the plasma temperature is low and the density is high, however, the collional process plays important role to make the quivering motion random. This is the thermalization of the electrons or the heating process of the plasma by the inverse-bremsstrahlung mechanism. More detailed description is given, for example, in the textbook by Kruer.[17] If the laser intensity is not so high (say, less than 10^{13} W/cm^2), the absorption process and the following physical processes become very complicated. However, such case has been studied relating to the industrial application of lasers such as material processing with laser ablation.[18]

For the case when the material is of low-Z, the absorbed laser energy is transferred into the over-dense region by the electron heat conduction as shown in Fig. 2(b). The heat conduction is nonlinear because the electron mean-free-path is a strong function of its temperature. And a heat wave is formed with its velocity decreasing rapidly as a function of time.[19] When the sound velocity of the heated region becomes comparable to the velocity of the heat wave, a shock wave is generated and propagates in front of the heat wave. On the other hand, the heated material expands into the vacuum with the velocity roughly equal to the sound velocity. The rear end of the expansion wave runs after the heat wave. Almost the same time as the shock wave is formed, the heat wave merges with the expansion wave to form the ablative heat wave. After this time, the structure seen in Fig. 2(c) is maintained under the constant irradiation of laser. For the case of the laser intensity of about 10^{14} W/cm^2, the time scale for changing from Fig. 2(b) to Fig. 2(c) is several pico-seconds. Therefore, it is a good approximation to assume that the structure of Fig. 2(c) will be kept through the laser irradiation as long as the pulse duration is much longer than this time scale.[20]

In the case when the solid material is of high-Z (e.g., gold), most of the absorbed energy is converted to soft X-rays in the conduction region.[21] Then, the heat wave

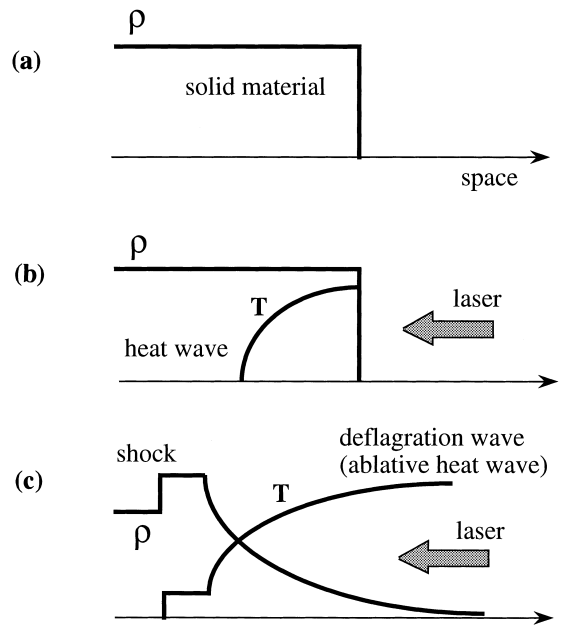

Fig. 2. Schematic pictures of density and temperature profiles in very early time, when an intense laser is irradiated on a solid surface. (a) Initial state. (b) Nonlinear heat wave propagates into the solid material without hydrodynamic motion. (c) In later time, a shock wave is generated by the deflagration wave sustained by continuous heating by laser.

and the ablative heat wave in Fig. 2 are sustained by the X-ray radiation. The X-rays escape from the plasma toward the right in Fig. 2, and almost 70–80 % of the absorbed energy is released into vacuum as X-ray energy. The spectrum of the X-rays is near the Planckian distribution. Since the thermal X-rays are generated mainly in the conduction region, the temperature of the radiation is almost same as the temperature of this region. The radiation temperature is usually a few hundreds eV.[22] By irradiating the lasers inside the cylindrical cavity of gold, we can confine the X-rays in the cavity to produce a Planckian X-ray source.[23] This cavity is called "houlraum" and has been widely used in the scheme of radiation driven inertial confinement fusion.[15] The cavity X-ray has also been widely used to drive strong shock waves to measure the equation of state, to heat the sample material for the opacity experiment and so on.[1] The former two will be described more detail later. It is noted that even in the case of the laser irradiation on low-Z materials, several to ten percents of the absorbed energy escape from the plasma in the form of X-rays. In the case of the low-Z plasmas, however, the most of the absorbed energy is finally converted to the kinetic energy of the expending plasmas.

As can be guessed from the above description, the intense lasers can be used to study high-energy-density (HED) physics. The high-density plasmas with the temperature up to a few keV can be produced with the size of sub-mm. Such parameter of the plasma is limited by the achievable pressure. The pressure generated at the ablation front is called "ablation pressure" and has been studied theoretically and experimentally from the early time of laser plasma research.[24] When lasers with the

intensity of 10^{13}–10^{15} W/cm^2 is irradiated on a solid material, the ablation pressure in the range of a few tens to a hundred Mega-bar is generated. This extremely high pressure can be used to generate a strong shock wave in gas or solids.

We can enumerate another ways to generate high pressure; for example, a shock tube and a high explosive. However, the typical pressure generated by the shock tube is several tens of the atmosphere. With the high explosive the pressure reaches a few hundreds kilo-bar, while the ionization of dense matters cannot be expected. This is easily understood from the fact that the chemical reaction releases the energy of a few eV per molecule and is not enough to ionize atoms. From such point of view, it is not exaggeration to say that the laser is only way to realize HED plasmas in the laboratory.

The X-rays generated from the high-Z plasmas can be used to heat a small sample material uniformly. Such X-rays have been also used for diagnostic purpose. There are two ways to measure the state and dynamics of plasmas. One is the "passive" way in which the X-ray or optical signals coming from the plasmas are measured.[25] The other is the "active" way in which X-rays generated by another lasers are used to diagnose the laser-produced plasmas or another lasers are used for diagnostics. A variety of active and passive ways can be designed in laser astrophysics experiment.

The X-ray back-lighting and side-lighting techniques are a standard method to measure the density (optical thickness) structure of laser produced plasmas. In Fig. 3, a schematic configuration of the X-ray side-lighting technique is shown. Figure 3 indicates the configuration to obtain the images of hydrodynamic instability growing in a plastic foil being accelerated by laser irradiated from the bottom side. A hard X-ray is generated by another laser beam irradiated on an X-ray source material. The transmitted X-ray is measured by the time resolved X-ray imaging camera as shown in Fig. 3.[26] A typical example of the X-ray transmitted image is shown on the left in Fig. 3. The target foil is located initially near the bottom in the image and, then, accelerated upward. The target surface was corrugated to provide an initial perturbation for Rayleigh-Taylor instability. It is seen in the shadow image in Fig. 3 that the perturbation has grown into the nonlinear phase, where the initial sinusoidal perturbation has become the bubble-spike structure. The perturbation has already penetrated into the rear side of the target, where perturbed structure is also seen. Details of the linear growth rate of R-T instability was measured by analyzing the time evolution of the intensity of the transmitted X-ray through the target foil.[27] More details on the diagnostics and the experimental result of RT instability growth are given, for example, by Remington et al.[28] and Azechi et al.[29]

Relatively hard X-ray from plasmas can be used to measure the interior of the plasmas. For example, the time evolution of the compressed core has been measured by a multi-imaging X-ray streak camera (MIXS) in multi-beam laser implosion experiment.[30] The temporal resolution of the time-resolved imaging has been improved to be better than 10 ps, and is sufficient to measure the implosion dynamics whose time scale is 10–100 time longer than this resolution limit. The line X-rays are a good signal to measure the ionization stage of plasmas. For example, an X-ray monochromatic camera has been developed to study the temporal and spatial evolu-

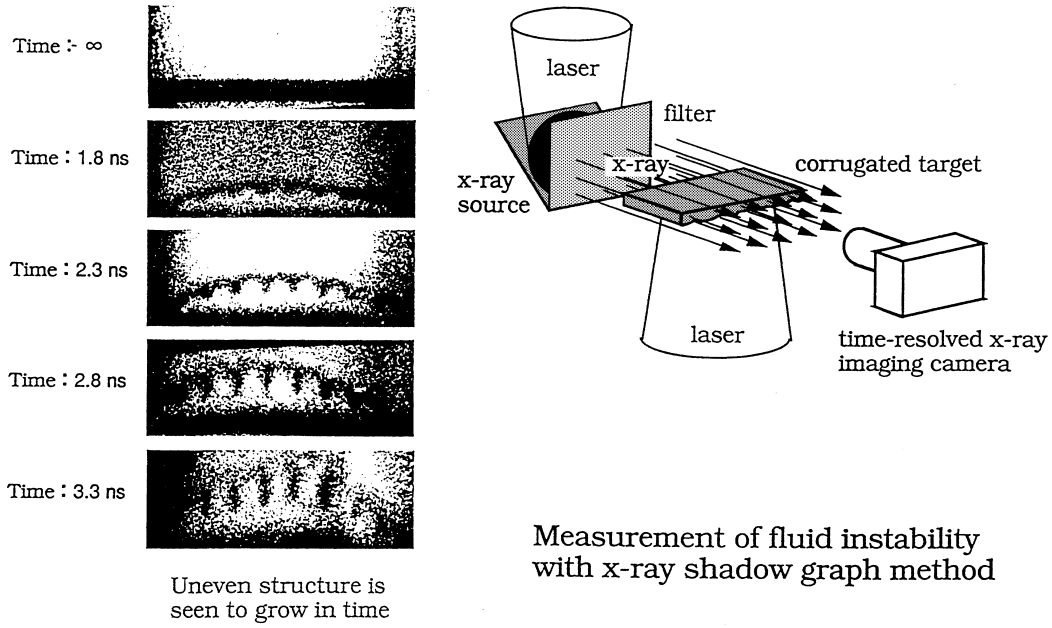

Fig. 3. The principle of X-ray sidelight imaging technology is shown on the right for the case when the corrugated foil is accelerated by laser from the bottom side. A typical example of time sequence of the transmitted X-ray image is shown on the left, where the growth of Rayleigh-Taylor instability is clearly seen.

tion of compressed core plasmas.[31] Seed materials are mixed or doped in a target for diagnostic purpose. The line X-rays from the seed materials are measured, for example, for studying the time evolution of the compressed gas fuel. Such diagnostics has been intensively used to check a computational modeling of material mixing due to the hydrodynamic instability.[32]

§3. Hydrodynamics and shocks

The rear of the shocked, high-dense region in Fig. 2(c) is called "ablation front". The region from the ablation front to the point of laser absorption is called "conduction region" or "deflaglation region". The deflagration is the name for a slow combustion wave front.[33] If we regard the laser heating as the energy increase due to chemical reaction in the combustion, we can also use this word for the case of laser heating. In Fig. 4, the change of the pressure and specific volume is plotted to explain the change of thermodynamic state in laser produced plasmas. The points 1, 2, and 3 represent the un-shocked solid region, shocked region, and the rear of the deflagration wave roughly defined to be the laser absorption point. The point "1" jumps to the point "2" according to the Ranking-Hugoniot (R-H) relation. In general, the solid target is not subject to the ideal equation of state (EOS). The realistic EOS should be modeled, for example, in simulating such hydrodynamics.[34] Then, the state of the plasma changes from the point "2" to a point of the deflagration-detonation curve (DD). In general, the Chapman-Jouguet deflagration is realized so

that the point "3" is the tangential point of the line from the point "2". The DD curve is located far above the R-H curve, because of the increase of the entropy of plasma in the deflagration region. In the deflagration region, the density decreases very rapidly by two to three orders of magnitudes and, in contrast, the temperature increases rapidly by the same orders. It should be noted that the point "3" must be very far from the point "2" in the measure of the specific volume, while the pressure is kept almost constant and decreases about to a half of the pressure at the ablation front. [20)]

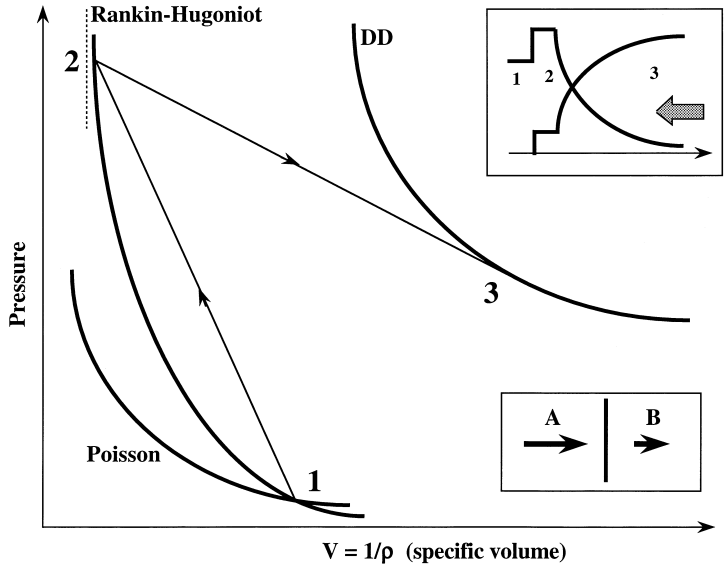

Fig. 4. Pressure and specific volume diagram of the stationary deflagration structure given in Fig. 2(c) or the figure of the right-top in this figure. The state "1" is the initial solid state and jumps to the state "2" in the shocked region and then expand to the state "3" at the heating point.

3.1. *Equation of state*

By use of the strong shock wave generated by the intense lasers, we can study the equation of state (EOS) of a variety of materials over their sold density. The ablation pressure generated by intense lasers reaches several tens Mega atmospheric pressure and it is comparable to the pressure near the center of giant planets like Jupiter. There has been a lot of discussion on the insulator-metal transition of hydrogen in the interior of Jupiter. By use of intense lasers, we can provide experimental data for studying the internal structure of giant planets, and such data can also used to study the properties of brown dwarfs.

The EOS is one of the important ingredients in simulating the hydrodynamics of laser-produced plasmas. [34)] A clear difference has been demonstrated by simulating a simple case, where an intense laser is irradiated on a solid aluminum foil. [35)] Since the generated pressure is over 10 Mbar, strong shock waves propagate in the solid aluminum. When the ideal gas assumption is used in the code, the density jump at the shock front is four times and strong compression is seen. In case where

more realistic EOS given as Los Alamos SESAME table[36] is used, in contrast, the resultant compression by the shock is relatively week. This fact is easily inferred with the fact that the bulk modulus of the solids tabulated, for example, in Table 4 of the textbook by Kittel[37] are very high. The bulk modulus is the pressure need to compress the solid to the half of its initial volume and the typical value is 5.45 Mbar for carbon and 0.722 Mbar for aluminum. It is important to model the Fermi pressure and molecular bonding and the molecular bonding should give the same bulk modulus as material data. The SESAME table is generated at first based on Thomas-Fermi statistical model[36] to the average ion. It is a good model in extremely high density compared to the solid density, while in our case the molecular bonding effect affects the results very much. In the SESAME table, the Thomas-Fermi model is modified with the addition of molecular bonding model based on the Morse type potential. In addition, this result is modified so that the table reproduces the experimental data, most of which are taken from the underground nuclear explosion tests.

The intense laser has been used to measure EOS over the solid density at extremely high pressure. The diagnostic technique has been established recently and applied to measure the shock Hugoniot relation of solid hydrogen. The solid hydrogen is produced by cryogenic system and two sides of almost cubic solid hydrogen are sustained by sapphire windows. An intense laser is irradiated on the aluminum foil, which is used to sustain the solid on the top, to generate a strong shock wave. Then, another laser beam is used to generate hard X-ray to be used for diagnosing the trajectory of the shadows of the shock front and the contact surface of the aluminum pushing the shock forward as shown in Fig. 5.[38] Another week laser beam is also used to measure the conductivity of the shocked region. More details are given in Ref. 38).

By knowing the velocity of the shock front U_s and the velocity of the contact surface which is equal to the particle velocity of piston velocity U_p, we can obtain the

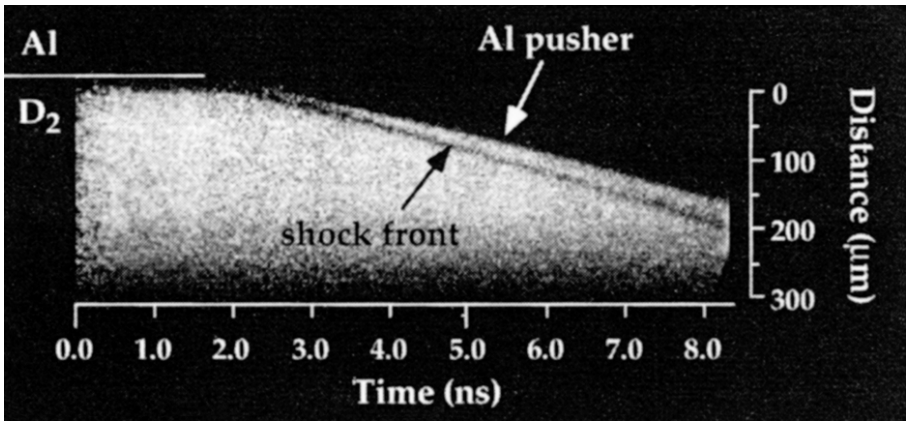

Fig. 5. X-ray sidelight image of traveling shock wave front in a solid deuterium and aluminum piston accelerated by laser irradiation. This raw data give us the Hugoniot relation of a strong shock wave.

pressure P and the density ρ of the shocked region by use of the following relation:[39]

$$P - P_0 = \rho_0 U_s U_p, \tag{1}$$

$$\rho/\rho_0 = U_s/(U_s - U_p), \tag{2}$$

where ρ_0 is the initial solid density and P_0 is the initial pressure. The resultant Hugoniot curve is shown in Fig. 6.[40] In Fig. 6, the experimental data are shown with solid circles with error bars, where the data taken from the gas gun experiments[41] are also shown with triangles at 20 Gpa (0.2 Mbar). In Fig. 6, the Hugoniot curve obtained with the SESAME table is plotted with a solid line, while that obtained with linear mixing model by Ross[42] is plotted with the other solid line. It is clear that the experiment shows higher compressibility than the SESAME predicted and the Ross's theoretical model predicts better Hugoniot curve to explain the experimental data. In Fig. 6, another theoretical curve which predicts a rapid change of the curve stemming from the first-order phase transition is also shown (Saumon & Chabrier; SC). However, there is no evidence for the first-order phase transition in the experimental data. The linear mixing model by Ross assumes that the Helmholtz free energy of the dissociating mixture is a function of linear combination of the free energy of the pure molecule and metallic hydrogen. The fact that the Ross's model

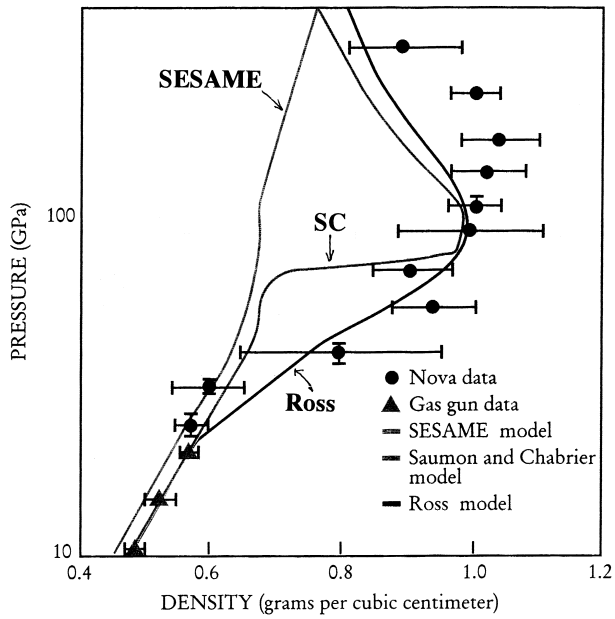

Fig. 6. Shock Hugoniot data taken from the experiment of Fig. 5. The experimental data are plotted with solid circle with error bars. The frequently used SESAME table of LANL does not fit the data. Nor a theoretical curve by Saumon and Chabrier (SC), which predicts the occurrence of the first order phase transition near the pressure of 60–70 Gpa, give a correct explanation of the data. The thick solid line by Ross rather well fits to the data and this fact indicates that the first order phase transition is not seen and the mixed state of molecule and metallic deuterium states continuously changes from the former to the latter. It also should be noted that the solid deuterium is much softer than expected with SESAME table previously.

can fit the experimental data suggests that the metallic-insulator transition is continuous along the change of pressure.

The higher compressibility near the solid density is a good news for laser fusion, because a target can be compressed with less pressure. At the present time, more detail experiments are in progress. One example is that being done at LULI, Ecole Politechnique,[43] France as a joint research with Rutheford-Appleton Laboratory in UK. In this experiment, diamond anvil cell is used to compress the solid deuterium up to 0.1 Mbar. In near future, the different Hugoniot curve with different initial conditions will be plotted in Fig. 6. In addition, it will be informative to let you know that laser reflection method coupled with interferometric technique is now used to study EOS of water at LULI.[43]

The EOS study is a good and easy-to-understand example to relate laser-plasma to astrophysics and planetary physics. This comes from the first point of the three viewpoints, "Sameness" of physics, regardless the size of plasma.

3.2. *Strong shock matter interactions*

The physics of the interaction of strong shock waves and the interstellar medium (ISM) is important, for example, to study the evolution scenario of stars. A strong shock wave generated by supernova explosion expands over a long distance in a galaxy. The shock compresses the ISM or more dense molecular clouds, consequently triggering the formation of many stars. As explained in Appendix C, the vortexes are also generated when the density gradient of ISM or molecular cloud is not in parallel to the direction of the shock propagation. Such formation of vortex is also important to understand the morphology of supernova remnants, for example, a bullet-like structure of a small portion of the supernova remnant known as the Cygnus Loop, whose Hubble Space Telescope (HST) image is given, for example, in Ref. 44). The supernova shock has collided with a dense interstellar gas, heating the gas and causing it to glow.

A variety of numerical simulations has been carried out, on the other hand, to understand the details of fluid dynamics and vortex formations observed when a shock wave collides with density discontinuity.[45] As explained in Appendix C, the linear phase of this dynamics is known as Richtmyer-Meshkov instability and has been studied intensively in a variety of research fields including ICF.[46] In the field of shock tube experiment, time evolution of a small bump on a plane surface was observed with laser sheet imaging techniques and compared with the corresponding large-scale simulation in two or three dimension.[47),48] It is demonstrated that the hump grows in size as dip in later nonlinear stage and three-dimensional effect becomes important. In the nonlinear stage of the Richtmyer-Meshkov instability, strong shear flows appear along the deformed discontinuous surface and Kelvin-Helmholtz instability causes vortex line on the contact surface to break up.[49),50] Such shock tube experiment is very useful to discuss the morphology of shock-clump interaction in the universe from hydrodynamics point of view.

In the case of astrophysical phenomena, the fundamental physics as fluid dynamics can be studied by such shock tube experiments. In general, however, the shocks collide with ISM with its Mach number more than ten. Therefore, the physics has

been studied mainly by computer simulation.[51] In the case of plane shock and dense sphere interaction, the baloclinic term described in Appendix C causes the generation of a vortex-ring surrounding the equator of the sphere. In the later nonlinear phase, it is well known that this ring becomes unstable to $m = 5$ mode perturbation. Three-dimensional effect becomes essential in morphology of the shocked-matter.[51] A model experiment of Mach 10 shock-matter interaction physics has been carried out with NOVA laser system at LLNL.[52] The observed trajectory of the shock is compared with simulation, concluding a good agreement. The time evolution of the density distribution of the optical thickness of a plastic sphere used to model the shocked-ISC (inter-stellar cloud) has been observed by X-ray back light method. The experimental data are compared to two simulation results; one is obtained with axially symmetric two-dimensional code, CALE, and the other is done with three-dimensional code with AMR (adaptive-mesh refinement) technique. In Ref. 52), the bifurcation of the vortex ring is observed only in the experiment and 3D AMR code, while the 2D CALE provides unphysical solution indicating a long last of the vortex ring. More detail 3D simulation has been carried out recently with HYDRA 3D code originally developed for ICF target design.[53] For this simulation, the world fastest computer "White Pacific" at LLNL has been used and a quite long time CPU is used in the framework of ASCI (Accelerating Strategic Computing Initiative) project.[54]

It is clear by comparing the optical and X-ray image of the whole structure of Cygnus Loop supernova remnant (SNR), the X-ray emission is much stronger than the optical. The temperature after the shock passage increases very drastically and matter is ionized. This is more drastic in case of a very young SNR such as supernova (SN) 1987A. It is well known that SN1987A has triple rings and the inner ring with the diameter of 1.3 light years is recently heated up by the collision of shock wave by the ejecting material from SN1987A,[55] the velocity of which is about 5,000 to 10,000 km/s. It is seen that several knots in the gas ring around the SA1987A are brighten in the optical image of HST due to the shock wave. In addition, the recent Chandra X-ray image indicates that the previously-unseen material inside the optical ring is heated to several 100 eV and emitting X-ray.[56] The peak intensity of the X-ray is near the peak of the optical image and the shock is heating the ring gas and the total X-ray luminosity is increasing.

In such young SNR phenomena, not only the hydrodynamic phenomena but also non-LTE (Locally Thermodynamic Equilibrium) atomic process becomes important in a strong-shock matter interaction physics. A preliminary model experiment has been carried out with GekkoXII laser.[57] The two-dimensional simulation has also carried out to design and analyze the model experiment.[58] The simulation provides the peak temperature in the optical ring about 700 eV and the initial ionization phase and the later recombination phase are both not in LTE. For detail modeling, the non-LTE atomic process becomes important as described in §5.

§4. Hydrodynamic instabilities

4.1. *Laser implosion and SN1987A*

The hydrodynamic instability is the most important issue in laser implosion. By the mid-'80s, we have concluded that the Rayleigh-Taylor instability in the final compression phase is uncontrollable and the final compression seen in 1D code cannot be expected.[59] This has been concluded by a series of implosion experiment with DT (Deuferium-Tritium) gas-filled glass micro-balloon targets. In Fig. 7, the experimental neutron yield and 1D simulation yield per input laser energy of 10 kJ are plotted as a function of the target aspect ratio, defined by the initial radius divided by the glass thickness, with the solid circle and ⊞ marks, respectively.[59] It is seen that even at the best fit the experimental yield is a half of 1D yield and this discrepancy increases as the aspect ratio reduces. This discrepancy is due to the Rayleigh-Taylor instability at the final stagnation phase.[60] The decrease of the aspect ratio means the increase of the glass shell thickness and the larger fraction of heavy glass material remains at the stagnation phase. This causes the Rayleigh-Taylor instability at the contact surface of glass and DT fuel, and the increase of neutron yield in this phase cannot be observed in the implosion experiment. This is our understanding at the stage of the mid-'80s.

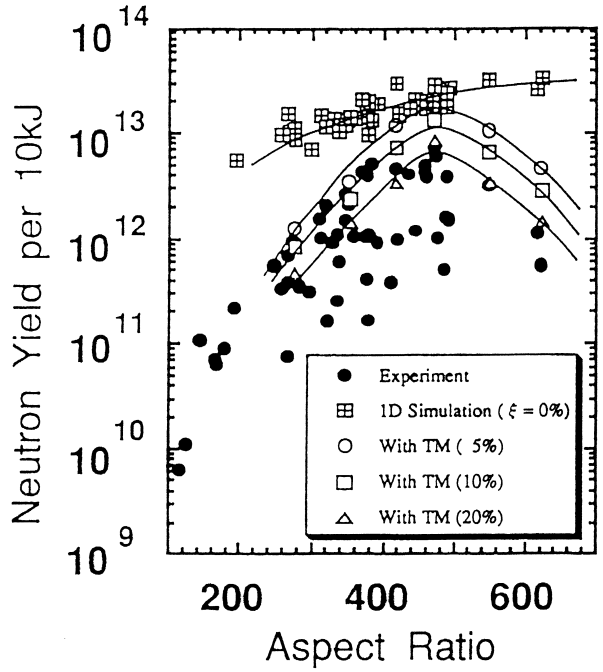

Fig. 7. Experimental data (solid circles) of many implosions of glass micro-balloon target filled with DT fuel. Comparison of these data to those one-dimensional simulation results (⊞ marks) leads us to the conclusion that a hydrodynamic mixing driven by Rayleigh-Taylor instability quenches the more fusion reaction in the final compression phase. This hypothesis is backed by the result with simulation including a mixing model.

As already touched a bit in the previous section, I think the readers well know Supernova 1987A (SN1987A) the explosion of which was observed on February 23, 1987. This was a spectacular event able to be described as "the experiment by God" at the time when modern instruments are ready to observe the details of the explosion. The SN explosion at such near distance, only 160,000 light years, was the event after an interval of 400 years. Throughout the research related to SN1987A, I understand that three remarkable accomplishments have been achieved. One is that the theory of gravitational collapse has been approved. The second is the observation of 12 neutrinos in a pure water tank at Kamioka, Japan, and it led to the present big topics of neutrino oscillation. The third one is the fact that the explosion is not spherically symmetric, while the hydrodynamic instabilities cause the convection of the inner and outer layers, consequently mixing the outer H/He layer with the inner heavy metal.[61)]

The third point has been concluded through the research to explain the hard X-ray emission from SN1987A, which is observed by Japanese X-ray satellite, "Ginga". In Fig. 8, the time evolution of the X-ray luminosity in the range of 16–28 keV is

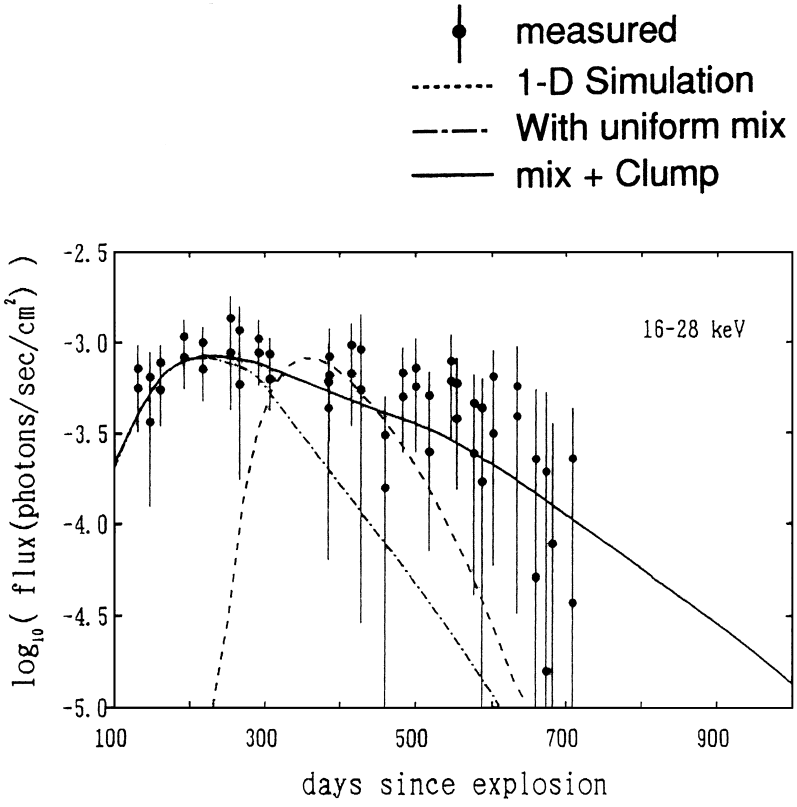

Fig. 8. Comptonized X-ray signal observed from SN1987A by Japanese X-ray satellite "GINGA". The data with error bars are observed ones, while simple one-dimensional explosion simulation given with dashed line did not explain the observed data. The simulation assuming uniform mixing could explain the early behaviour of the data, while additional inclusion of clumpy metal is required to explain the data with satisfaction as shown by the solid line.

plotted. The data with error bars are those observed by "Ginga", while the other three lines are theoretical ones. This X-ray is the X-ray produced by softening of the line γ-rays generated by the nuclear decay of ^{56}Ni to ^{56}Co and to ^{56}Fe. Then, the line γ-rays of about 1 MeV are emitted. The ^{56}Ni is predominantly nucleosynthesized deep inside of the layered massive stars, when a strong shock wave generated by the gravitational collapse passes through the ^{28}Si layer. These MeV γ-rays by nuclear decays are Compton scattered many times and soften to hard X-ray. Since the optical thickness of the outer layer is thick and decreases as the matter expands, the hard X-ray escapes out after a certain time from SN explosion.

Although one-dimensional code predicted the appearance of the X-ray will be almost one year after the explosion as plotted by the dashed line, "Ginga" satellite began to observe the X-ray about 100 days after the explosion. Most probable candidate to explain the discrepancy is the mixing of materials due to hydrodynamic instabilities,[61] similar to the case of laser implosion in Fig. 7. An empirical mixing model has been installed in a 1D code, and a Monte-Carlo calculation has been carried out to explain the data by "Ginga".[62] The result is shown with the solid line in Fig. 8. In Fig. 8, the dash-dotted line represents the result when only molecular scale mixing is taken into account, while the solid line represents the result when not only the molecular but also clumpy scale material mixing is also taken into account. From Fig. 8, it is concluded that not only micro-scale mixing but also macro-scale mixing are of general feature of the gravitationally collapsing Type II supernova explosion.

This analogy of the physics in laser implosion and SN1987A explosion became the trigger for the author to develop the new field of laser astrophysics described in this paper.

4.2. *Instabilities in three phases in Type II SN explosion*

In the explosion of Type II supernovae, there are three phases in which hydrodynamic instability becomes critical in evolution scenario. As shown schematically in Fig. 9, one is the very early phase around one second after the gravitational collapse, the second one is the early phase in the scale of a year, and the third is the SNR phase in the year of thousands. In Type II supernovae, the central iron core whose mass is about the solar mass and radius is about 1000 km gravitationally collapses to form a proto neutron star with the radius of about 10 km. Most of the gravitational energy released due to the collapse is converted to the energy of neutrino. As shown in Fig. 9(1), the neutrino heats the outer layer consisting mainly of silicon and re-births the shock wave originally generated by a bounce of the collapse ["SW" in Fig. 9(1)]. This shock wave propagates to the surface of the star in about two hours and the light from the heated surface is observed as supernova explosion. In this very early phase after the collapse, the inner surface which appeared by iron-core collapse becomes unstable to Rayleigh-Taylor instability.

It is widely accepted that the neutrino heating is not sufficient to re-birth the shock wave in one-dimensional simulation. The shock wave initially generated by the bounce loses its energy in propagating the silicon layer because of the heat-absorbing nuclear reaction. In order for the neutrino to supply the sufficient energy to the

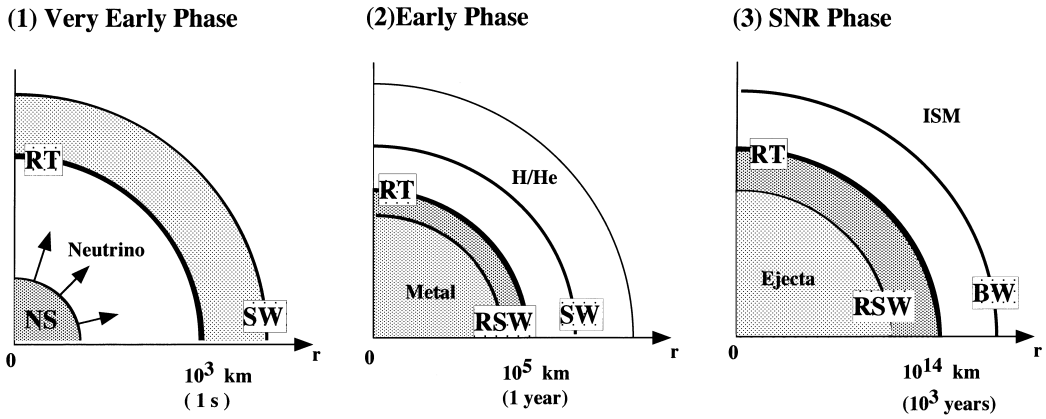

Fig. 9. Three phases of Type II supernova explosion where hydrodynamic instability becomes essential subject to be studied. The first is very early phase just after the central iron core is gravitationally collapsed and the proto neutron star is formed. In this case, the outer surface of the collapsed core region becomes unstable to Rayleigh Taylor instability. In order to re-birth the shock wave propagating outward, efficient convective mixing in this unstable region is required. The second is an early phase in the range of days to a year. In this case, the contact surface between heavy metal layer (hatched region in Fig. 9(2)) and H/He layer (white region) is once accelerated outward by the shock wave by the explosion. Then the reflected shock (RSW) forms a pressure profile decelerating this surface. This pressure profile is strongly related to the spherical divergence of the physical quantities. Then, the contact surface becomes unstable to Rayleigh-Taylor instability. This phase is that important in Fig. 8. The third phase is in very later phase, so-called supernova remnant phase. About 400 years after the explosion, a blast wave is formed and the contact surface between the ejected material (shaded region) and the interstellar medium (ISM) tends to decelerate and becomes unstable to Rayleigh-Taylor instability.

shock wave, material convection near the surface indicated with "RT" in Fig. 9(1) is required in several seconds after the collapse.[63] Since the mean free path of the neutrino is extremely long even compared to the radius of the star, the non-local energy transport is essential in treating the transport of the neutrino. Therefore, we have to study the physics of Rayleigh-Taylor instability driven by a long-range energy carrier like neutrino. By replacing the neutrino with a long-range hard X-ray, we can design a model experiment with intense lasers.

In the model experiment, we convert laser energy to that of hard X-ray. When an intense laser is irradiated on a gold foil, the X-ray spectrum of the rear side of the foil is dominated by M-shell X-ray the mean energy of which is about 2.5 keV.[21] By impinging of this hard X-ray on a plastic foil and accelerating it, the foil becomes Rayleigh-Taylor unstable under the condition of non-local heating. In this model experiment, the same technique as explained in §2 (cf: Fig. 3) can be used for measurement. With such experiment, we can clarify general properties of the hydrodynamic instability driven by the non-local energy transport. In fact, the details of Rayleigh-Taylor instability driven by X-ray ablative acceleration has been studied intensively relating to the indirect drive ICF.[15),28),32)] In this case, however, some medium-Z material is doped to shorten the range of the coming X-ray and,

in addition, the hard component of the X-ray is eliminated so that the X-ray is efficiently absorbed and X-ray transport becomes rather local. It is useful to point out that the model experiment mentioned above will also be a model experiment of hydrodynamic instability driven by the alpha-particles generated at the central spark in the compressed and structured high-gain DT fuel core in ICF. The fire-polishing effect by the non-local transport of the alpha-particles has been demonstrated by 2D simulation.[64)]

In Fig. 9(2), the second stage of the early phase is schematically shown. In this phase, the re-birthed shock wave propagate through the onion-like structured outer layers. It is noted that the progenitor, the star before explosion, has a layered structure from the central iron to the outermost hydrogen. According to the papers,[65)] the contact surface between the shaded metal region and white H/He region ["RT" in Fig. 9(2)] is once accelerated outward impulsively by the passage of the shock wave. Then, it is continuously decelerated due to the pressure gradient made by the forward shock wave "SW" and the reverse shock wave "RSW" shown in Fig. 9(2). In this later phase, the heavy metal region is decelerated by the lighter H/He layer, and consequently the contact surface becomes unstable to Rayleigh-Taylor instability.[65)] Within a year, the instability develops into the nonlinear stage. This is the hydrodynamic instability and mixing described previously in §4.1 relating to Fig. 8. In this Rayleigh-Taylor instability, the effect of expanding spherical geometry and the seeding by impulsive Richtmyer-Meshkov instability to highly nonlinear Rayleigh-Taylor instability are interesting topics even as a basic research of the instabilities. In addition, there is still unsolved problem; namely, starting simulation with random perturbation, the unstable mode with the spherical wave-number $l = 20$ remains predominantly in the highly nonlinear stage. This may not be a special case of SN explosion, and would provide us with a theme of fundamental study.

A model experiment on the grow of the instability in the phase of Fig. 9(2) has been carried out by LLNL team with OMEGA laser at LLE, University of Rochester.[66)] In this experiment the geometry is a half cylinder with the central void, 85 μm thick copper hemicylinder with 400 μm inner diameter with 5 μm plastic ablator on the interior. The Cu hemicylinder with corrugated surface is mounted on 800 μm thick plastic layer. The heavy Cu layer and light plastic layer model, respectively, the metal and H/He layers of SN explosion. Six beams of OMEGA laser system are irradiated at the central interior surface to model SN explosion, and another two beams are used for back-lighting. In Fig. 10, two different evolutions of hydrodynamic instabilities are shown. The left is two-dimensional simulation of SN1987A,[67)] while the right is the experimental data. It is noted that the time and space scales are different by factor of about 10^{13}. In the experiment, at 75 ns the bubble-and-spike structure is clearly seen; while the structure is quite different from the 2D result of SN1987A. It is too early to say that some physics is missing, because the equation of state (EOS) alters the spike structure slim compared to the ideal EOS case. In addition, the initial density distribution is different. For example, the density of H/He layer of SN1987A decreases with the radius because of weaker gravity, while the density of plastic layer is constant in the model experiment. Even with such difficulty in model experiment, this data would be a good start to discuss

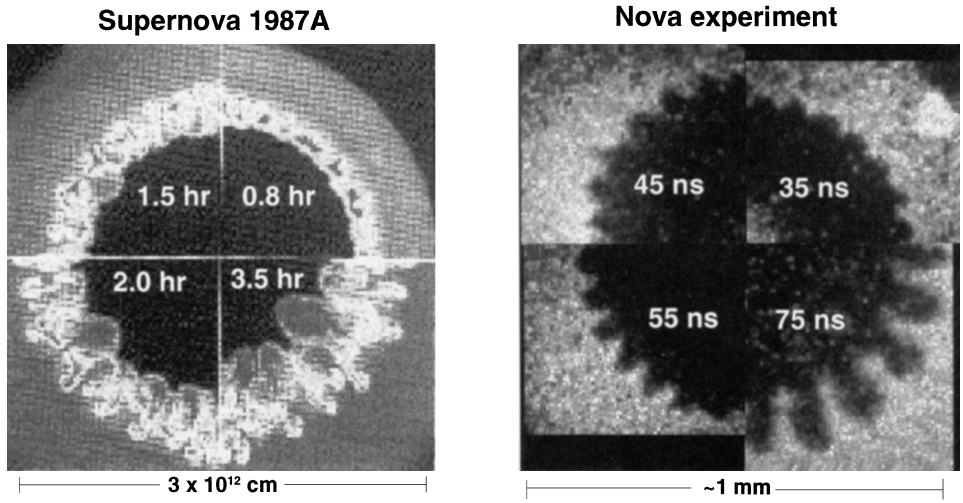

Fig. 10. Two dimensional simulation (left) and model experiment (right) of SN1987A explosion. Rayleight-Taylor instability evolves in the time of hours over the spatial scale of 10^{12} cm, while this evolution is modeled with NOVA laser at LLNL in the time and spatial scale 10^{-13} times smaller than the real system. It is seen that the spike-and-bubble structure clearly appears in the simulation and model experiment. The structures are different each other. This is a preliminary experiment and, for example, the density of the outer layer is constant in the experiment, while decreases with increase of the radius in the simulation. In addition, the experiment is not axially symmetric as the simulation, but hemi-cylindrical. In spite of such differences, however, such model experiment is useful to check the accuracy of the code used to simulate the supernova explosion.

the further elegant experiment.

In Fig. 9(3), schematic structure of supernova remnant phase after thousands of years is shown. Accompanying the SN explosion the ejecting material called "ejecta" expands into ISM with the velocity of about 10,000 km/s. During the first 400 years, the ejecta freely expand and accrete ISM at the front as snow plow. When the accreted mass becomes comparable to the mass of ejecta, the front of the ejecta begins to decelerate. Then, a blast wave "BW" is generated to propagate outward and the reverse shock wave "RSW" is also generated. The contact surface of the ejecta and ISM indicated with "RT" in Fig. 9(3) becomes unstable to Rayleigh-Taylor instability. Chevalier et al. have found self-similar solution of SNR in the phase of Fig. 9(3) and studied its linear stability[68] and carried out 2D simulations with and without radiation cooling effect.[69] According to the self-similar solution, the thickness between the contact surface and the reverse shock wave is kept less than 1/10 of the radius of the contact surface and the density of this thin layer is much higher than the both sides. Due to the deceleration force, the perturbation of the thin shell grows and finally shell-break happens. A typical simulation result is shown in Fig. 11, where the density structure is shown with the number of dots.[69] It is clearly seen that the contact surface becomes highly nonlinear. This instability is important to analyze, for example, the X-ray coming from SNR. If the shell is broken, the X-ray generated in the ejecta freely comes out. In general, metal abundance is different in

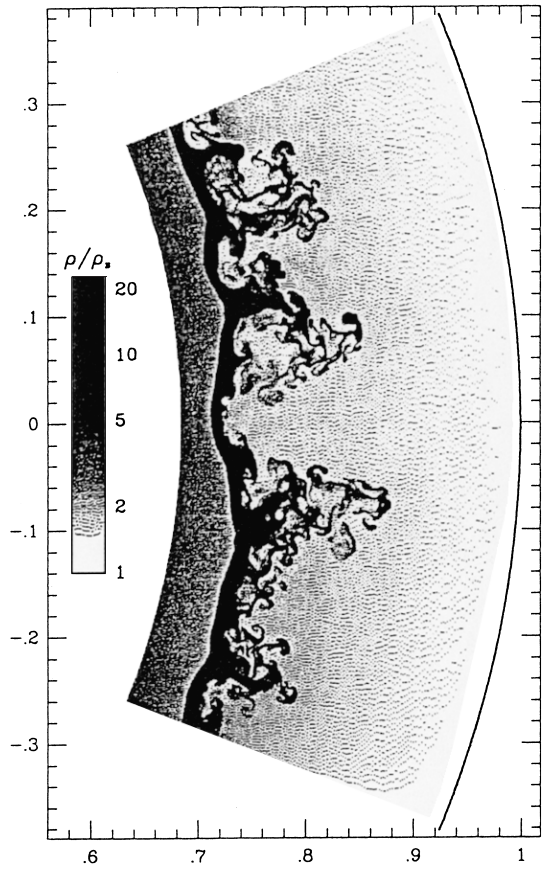

Fig. 11. Highly nonlinear stage of the hydrodynamic instability at the contact surface between the ejecta and ISM of SNR. The left sharp boundary is the deformed front of reversed shock wave front. The simulation is carried out based on a self-similar solution of spherically symmetric SNR. In the later stage, such fractal structure is kept almost frozen in the coordinate stretching according to the self-similar solution.

ejecta and ISM, and especially the line intensity is sensitive to whether seeing X-ray from the shocked ISM or ejecta. Finally, it is noted that the relative thickness of the shell and the distance of "BW" and "RT" are function of the effective specific heat γ. For example, radiation cooling or energy loss due to particle acceleration (source of cosmic rays) would reduce the effective γ and makes both thinner, consequently shell break-up or even the break-up of the blast wave front by the penetration of the spike of Rayleigh-Taylor instability becomes important.

4.3. *Hydrodynamic instability in Type Ia SNe*

Type Ia SN explosion is in general brighter than Type II SN explosion. Different from Type II SN, the most plausible progenitor of Type Ia is the white-dwarf in a binary system. The white dwarf consists of O/C and helium shell accreted from the atmosphere of the companion star. When the mass of the white dwarf becomes close to the Chandrasekar's limiting mass, 1.4 times the solar mass, Type Ia SN is

thought to explode. This is the reason why the Type Ia explosion is regarded as a standard candle in the universe to determine, for example, the Hubble constant,[70] its geometrical structure,[71] and the dark energy. The scale of explosion has been well studied with one-dimensional code with some mixing model. According such a model, the scenario of the explosion is as follows.

Due to the increase of the central density with the increase of the mass, the temperature increases to trigger the thermonuclear fusion of C-C and O-O. Finally, the carbon-oxygen are nucleosynthesized to become iron. Since the electron degenerate pressure is so high that the released thermal energy is not enough to generate a strong shock wave and the nuclear burning front remains as slow combustion wave (deflagration) for a while. If there is no mixing at the burning front, it remains as deflagration during the whole scenario and the most of the outer layer is expand before the burning wave reaches there. This expansion is driven by many of weak shock waves generated by the deflagration wave [see Fig. 2(c)]. In this case, Type Ia SN creates less amount of heavy element, especially iron, and this scenario is difficult to be accepted from view of explaining the abundance of metal in the universe. It is well accepted that Type Ia SN creates most of iron in the universe.

In order for Type Ia SNe to produce a large amount of iron, the most plausible scenario requires the change from the deflagration to the detonation before the burning front reaches the outer surface. In general, the deflagration (frame) front is unstable to Landau-Darrius (LD) instability.[72] In addition, the frame front is also unstable to Rayleigh-Taylor (RT) instability in this case. According to a simple model, we assume that the frame front grows to be fractal structure due to LD and RT instabilities and the total surface of the burning front increases with time. With the maximum wavelength $l_{\max}$ and minimum wavelength $l_{\min}$ of the front surface fluctuation, the total surface of the burning front A' is given in the form;[73]

$$A' = (l_{\max}/l_{\min})^{D-2} A, \tag{3}$$

where A is the surface of the burning front in the spherically symmetry and D is the fractal dimension and $D > 2$ in general.[73] Thanks to the increase of the surface, the burning rate increases proportionally to the surface area, and the effective burning front velocity V_{eff} is given in the form;

$$V_{\text{eff}} = (l_{\max}/l_{\min})^{D-2} V_{\text{cond}}, \tag{4}$$

where V_{cond} is the velocity of the one-dimensional deflagration wave determined by the thermal conduction. In the delayed detonation model of Type Ia,[74] it is believed that the deflagration wave changes to the detonation wave, when the effective burning wave velocity exceeds the local sound velocity.

It is critical to clarify the fractal dimension and the maximum and minimum fluctuation wavelengths in the present situation. In contrast to the one-dimensional scenario, if the burnig wave becomes detonation in the early time, almost whole of the white dwarf burns and too much iron is produced. The nature seems to require the medium scenario. There has been published a model calculation to determine the parameters in Eq. (4) by solving a master equation of imcompressible burning

front.[75] Within this simple model, the fractal dimension is not enough to enhance the velocity of the burning wave.

It seems to be difficult to do some model experiment of burning front instability with intense lasers, while the growth of RT instability in spherical geometry is common topics in both fields.

There are many works to understand the physics with large scale computing based on hydrodynamics in two-dimension or mostly three-dimension in these days.[76] It seems, however, that the smaller scale fluctuation appears, the smaller the grid size, and it is still open question how the instability grows and evolves into nonlinear stage and enhance the energy release by nuclear reactions.

In Type Ia SN explosion, we have to model the growth of the Rayleigh-Taylor instability coupled with the Landau-Darrieus instability. In the nonlinear stage, we can consider the statistical mechanics of the bubbles following the way developed by Don Shvart's group[77] and estimate the increase in the nuclear burning rate due to the increase in the surface area of the burning wave in the form of fractal structure. This model is coupled with the multi-dimensional explosion code to predict the scale of explosion. Such work originating the work done in laser fusion can be applied to identify the physical mechanism of the time evolution of the burning wave, which may change from deflagration wave to detonation wave.

4.4. *UV radiation driven Rayleigh-Taylor instability causing pillars of Eagle Nebula*

One of the great shots of HST (Hubble Space Telescope) is the gaseous pillars in M16, Eagle Nebula.[78] As for the origin of the pillars, Lyman Spitzer, Jr. wrote a paper in 1954.[79] His hypothesis was that the pillars are the remainder of the spikes produced by Rayleigh-Taylor instability driven by UV radiation from O/B stars near the pillars. This resembles the ablative RT instability in laser plasmas. Instead of lasers, the UV radiation is absorbed near HII boundary over which low temperature and high density molecular clouds exist. Through the ionization heating, the boundary moves with the pressure generated by the heating and is accelerated. Then, the boundary becomes unstable to RT instability and after a long time bubble and spike structure appears. It is usual in laser ablation case that the mushroom-type rolling up is not seen.[80] This is understood that the predominant heat conduction polish up a small scale-structure.[81] This seems to be the case of the pillars in Eagle Nebula.

Recently, detailed observation of the velocity distribution of the pillars has been carried out with radio wave.[82] The authors of Ref. 82) compared the data to the velocity profile predicted by a simple calculation of RT instability and concluded that the velocity distribution is not that predicted by RT theory; therefore the pillars are not due to the reason predicted by Spitzer. It is, however, too early to conclude so. One reason is that they used a very simple relation, (projected distance) $\propto$ (projected velocity)^2. This is nothing without a simple free falling theory and more detail analysis is required. It should be noted that this subject is well studied with 2D CALE simulation code of LLNL by J. Kane, and he reported that detailed simulation results show a good agreement with the velocity-distance relation.[83] It is interesting to do a model experiment on this subject, because in this case the RT instability is

not that of a simple contact surface, an ablating front stability should be studied. The same kind of stabilization mechanism as given by Takabe formula[84),85)] would be expected in the linear phase.

§5. Atomic physics and X-ray transport

Atomic physics is one of the key elements to model astrophysical phenomena and analyze observation data. Based on the view of the sameness described in §3, X-ray absorption and emission spectra of hot dense matter, essential ingredient in astrophysics, can be studied with laser produced plasmas. According to our custom, I would call these spectra as opacity in short.

5.1. *Opacity and opacity experiment*

The opacity has been studied with intense lasers from more than a decade ago and this experiment has been called "laser opacity experiment". Since the experiment can be done with relatively small scale lasers and more than ten codes for opacity calculation have been developed over the world, the detailed research became active.[86)] The opacity is the most fundamental physical quantity in discussing, for example, the evolution of stars. The energy generated by nuclear fusion around the center of the sun is transferred toward the outer layer by X-ray radiation. The energy transport rate is determined by the opacity of the plasma of the sun. Although the fraction of metal like iron is relatively small, the contribution to the opacity is relatively high. This is because the iron is high-Z compared to hydrogen and helium. The energy carried by the radiation transport near the surface is, then, transferred to the surface by convection. This is called Besnards convection, which is the same as Rayleigh-Taylor instability from the view of the physical mechanism. It is easy to infer that the temperature distribution in the sun is determined by the opacity. The detailed study of the internal structure of the sun is carried in the field of "helioseismology".[87)] OPAL code[88)] developed at LLNL has been used to analyze the data of helioseismology and it is demonstrated that the observation data are well reproduced within an error of a few % by use of EOS consistent with the opacity of OPAL code.[88)]

The opacity code has been compared with the data obtained with the laser experiment. Since the principle of the experiment is simple as shown in Fig. 12, I try to explain briefly the experiment. We need at least two laser beams. Let think the case to get the opacity of Fe. A thin Fe foil is sandwiched with thin plastic foils. Usually the X-ray generated by irradiating laser on a high-Z foil is shone on the Fe foil. The X-ray irradiated on Fe foil has a radiation temperature about 100 eV and only Fe is heated up to several 10 s eV. The plastic does not absorb X-ray and works as tamper to prohibit the expansion of Fe plasma. Thanks to this, we can realize high temperature and high-density plasma whose density is comparable to the solid density. At this time, X-ray generated by the other laser beam is designed to pass through the Fe plasma. By taking the ratio of the X-ray which passed the Fe foil and the same X-ray that did not pass through the foil, the spectral transmission is obtained. Since we know the initial mass thickness of Fe, the data can be easily

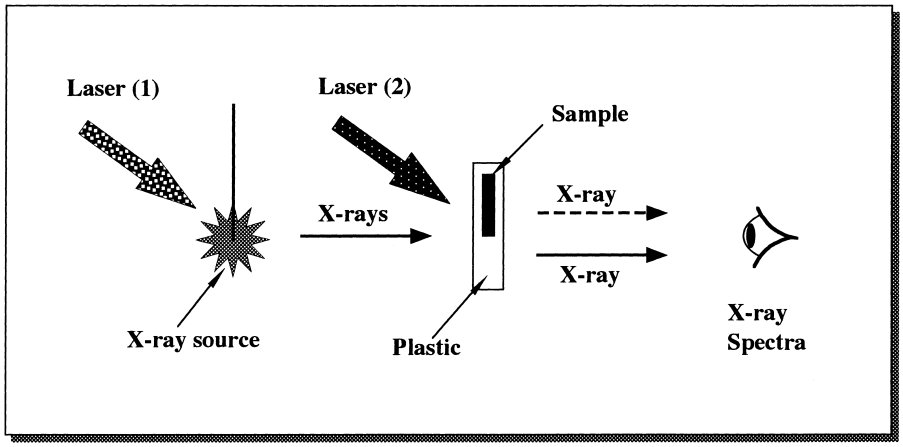

Fig. 12. A schematic picture of laser opacity experiment. The sample is tamped with plastic foil and irradiated by laser or soft X-ray produced by laser. Another X-ray generated by another laser beam is irradiated through the heated sample and X-ray crystal spectroscopy is used to compare the spectral intensities transmitting the sample and passing only the plastic layer. This ratio provides the spectral optical thickness of the sample plasma.

translated to the spectral opacity.[89]

Owing to the well-checked opacity, a big progress has been seen in astrophysics. Nova light curve is a good example where the opacity plays important role.[90] In order to get an image of Nova explosion, it is informative to see pictures taken by HST.[91] Nova is observed when one star in a binary pair dumps material onto the surface of the white dwarf, the other star of the binary. What we saw is basically a thermonuclear explosion that was triggered at the bottom of accreted material on the surface of the white dwarf. Nova Cygni 1992 was discovered from the ground and imaged by HST soon after its latest eruption. The image shows a ring of light and the central light surrounding a white dwarf. It is reported that the ring expanded 3.5×10^{10} km from the star in the intervening seven months. The expansion of the ring is very sensitive to the opacity of the ring. It is reported in Ref. 90) that the old opacity data are estimated lower by a factor two in the situation where the contribution from $\Delta n = 0$ transition in the M-shell of iron becomes important. Due to the increase of the opacity of the ring, the X-ray coming from the bottom are absorbed more efficiently by the ring, consequently enhancing the expansion velocity through increased pressure. Kato and Hachisu obtained a good agreement on the light curve for Nova, Cygni 1978 by using the table produced with OPAL code.[90]

Another good example is the Petersen diagram of variable Cepheids.[92),93)] This is the diagram made of the oscillation period of $m = 0$ mode (expansion and shrink spherically) and the ratio of the oscillation period of $m = 1$ mode expanded by Legendre function and that of $m = 0$ mode. Before OPAL code is used, the theoretical relation could not explain the observed data, while with OPAL the data have been well reproduced theoretically.

5.2. *Hydrodynamics of supernova remnants*

It is usual to use hydrodynamic equation to describe the phenomena in extremely low density ISM. This is good approximation because the spatial scale of the phenomena is extremely large and the justification parameter for hydrodynamic approximation, dimensionless parameter Knudsen number $K(=\lambda/L)$, is sufficiently smaller than unity. Here, λ is the mean-free-path and L is the scale length of change of physical quantities. The mean-free-path λ is given with the collisional cross-section σ and the particle number density n in the form: $\lambda = 1/(n\sigma)$. In general, the cross-section σ does not depend on the density and the following relation holds:

$$K = \frac{1}{\sigma n L} \propto \frac{1}{nL}. \tag{5}$$

In order to keep the Knudesen number constant, it is better to increase the density in case of laser plasmas.

If the condition $K \ll 1$ is satisfied, we can use hydrodynamic equations;

$$\frac{d}{dt}\rho = -\rho\nabla\boldsymbol{u}, \tag{6}$$

$$\rho\frac{d}{dt}\boldsymbol{u} = -\nabla P, \tag{7}$$

$$\rho\frac{d}{dt}\varepsilon = -P\nabla\boldsymbol{u} + \nabla\boldsymbol{q}, \tag{8}$$

where ρ is the mass density, $\boldsymbol{u}$ is the flow velocity, and ε is the specific internal energy, respectively. In Eqs. (6)–(8), P is the pressure, $\boldsymbol{q}$ is the heat flux. Depending upon a problem, the gravitational term, viscosity, or photon pressure will appear in Eqs. (7) and (8), and the heating and cooling terms in Eq. (8).

One of the characteristic points of the hydrodynamic equation is that if adiabatic condition is satisfied [$\nabla\boldsymbol{q} = 0$ in Eq. (8)], the following relation is universally satisfied from the dimensional analysis of Eqs. (6)–(8). The density ρ is independent and $u \sim r/t, P \sim \rho u^2$, where we assumed a relation $\varepsilon \propto P/\rho$. As is clear from this relation, we can do a model experiment by scaling down the phenomena in the universe.

The theoretical base for the similarity transformation is the existence of a self-similar solution. Regarding the astrophysics, we can enumerate, for example, Yahil solution [63] describing the accreting flow due to the gravitational collapse of a star, Sedov-Taylor solution [94] for the blast wave driven by spontaneous explosion of supernova, and Chevalier solution [68),69] for structured SNR already explained in the previous section. On the other hand, in laser produced plasmas we can enumerate, for example, Guderley solution [95] giving a spherically converging shock wave, Kidder solution [96] describing homogeneously imploding spherical target, and Hattori solution [97] describing the implosion dynamics in the final compression phase. More generally, the rarefaction wave and heat waves can be described with self-similar-solutions [98] and the self-similar method is very useful one to find an idealized solution of the nonlinear equations for hydrodynamics, energy transport, and so on.

Let us consider a spherically symmetric hydrodynamic flow. Let us assume that the spatial structure is given as a function of only the dimensionless variable

ξ defined as $\xi = r/R(t)$, where R is a function of time t and it is usual that the radius R depends on the power of t. In what follows, Sedov-Taylor solution is briefly explained to consider the dynamics of SNRs.

Regarding a supernova explosion as a spontaneous energy release of E_0 in the space of uniform density ρ_0, we find a spherically uniform solution of Eqs. (6)–(8). Let us assume the radius of the shock front generated by the explosion is given to be $R_{\rm BW}(t)$, and introduce the dimensionless radius ξ

$$\xi = \frac{r}{R_{\rm BW}(t)}. \tag{9}$$

By use of the energy conservation relation $\rho_0 R_{\rm BW}^3 (R_{\rm BW}/t)^2 \propto E_0$, we obtain the relation;

$$R_{\rm BW}(t) = \alpha \left(\frac{E_0 t^2}{\rho_0} \right)^{1/5}, \tag{10}$$

where α is an unknown dimensionless value and is given as the eigen value after solving equations.

More detail is given, for example, in Ref. 94). In assuming that the radial structure of the blast wave is given only as a function of ξ, we can reduce Eqs. (6)–(8) to coupled ordinary differential equations to ξ. By solving these equations so that they satisfy appropriate boundary conditions, we can determine the value of α and obtain the solution. For convenience, the structure for the case where the relations $\varepsilon = (\gamma - 1)^{-1} P/\rho$ is satisfied with $\gamma = 5/3$ is given in Fig. 13. In this case the value of α is obtained 1.17. It is surprising that the value of α is very near unity. In Fig. 13, at the front ($\xi = 1$), the strong shock jump relation is satisfied,

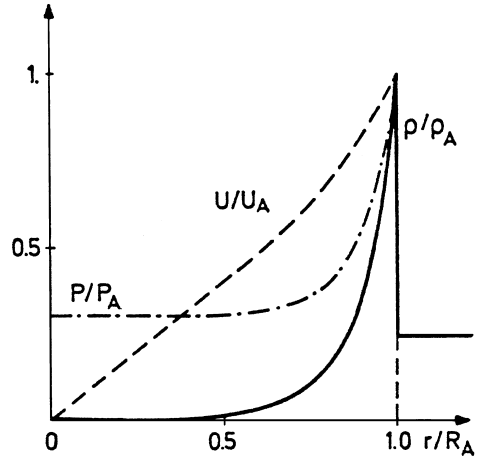

Fig. 13. Normalized structure of the blast wave for the case with the specific heat $\gamma = 5/3$. The definition of the radius of the blast wave $R_{\rm A}$ is given in Eq. (10). At the front, strong shock wave relation is used. Because of the spherical effect, the density drops down to zero at the center, and the velocity should also vanish at the center because of the boundary condition. The pressure increases abruptly at the blast wave front and then drops again in the rear side of the front.

and the density and flow velocity tend to vanish at the center. This means that the temperature is infinity at the center. In fact, the thermal conduction by radiation appears to be important at the center and keeps the temperature finite.[99] It should be of course noted that the self-similar solution provides an idealized solution and details are different.

Let us insert the typical values of supernova explosion; $E_0 = 10^{51}$ erg, $\rho_0 = 2 \times 10^{-24}$ g/cm^3 (about one proton per cm^3). Then, at time of 10^3 years ($= 3 \times 10^{10}$ s), $R_{\rm BW}$ is obtained to be 10 ly ($= 10^{19}$ cm), where ly is the light year distance. For these parameters, the relation of Eq. (10) is plotted in Fig. 14 with the line (A). On the other hand, the case of the intense laser with parameters, $E_0 = 10$ kJ and $\rho_0 = 2 \times 10^{-6}$ g/cm^3 (about 10^{-3} atmospheric gas), is plotted with the line (B). From the dimensional analysis, the temperature is proportional to the $(r/t)^2$ and the line for a constant value of r/t is plotted from the (10^3 years, 10 ly) point of supernova to the case of laser blast wave. In this case, the same temperature is seen in the blast wave of 1 cm in radius at 3 ns as shown in Fig. 14.

There is an interesting story on the Sedov-Taylor self-similar solution. It is well known that atomic bombs have been constructed at Los Alamos in the Manhattan project. The world-first A-bomb demonstration was carried out in New Mexico.

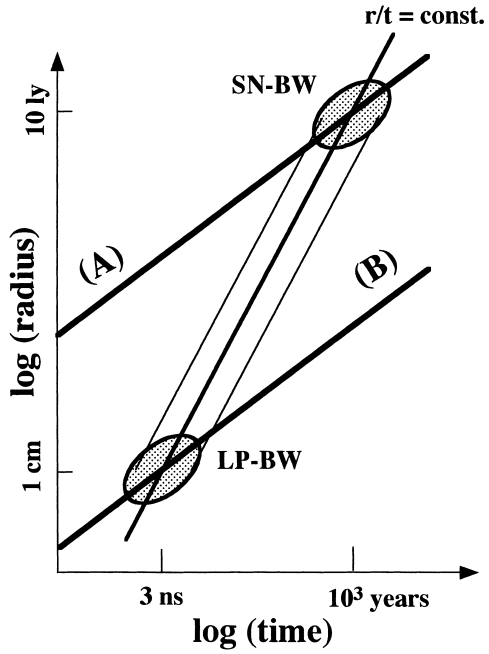

Fig. 14. The relation of Eq. (10) is plotted for two cases. One is the case of supernova blast wave (SN-BW). The other is the case of laser-produced blast wave (LP-BW). In plotting the curve, typical parameters are given for the explosion energy E_0 and the density of the surrounding gas ρ_0. If we require the same temperature history, the crossing points of both lines with the same r/t value satisfy the requirement. This means SNR with the size of 10 ly and the age of 1000 years is reproduced with the laser-produced plasma whose size is 1 cm at the time of 3 ns after the laser irradiation. The scale of time and space is transferred almost a factor of 10^{19} in this similarity transformation.

Professor G. I. Taylor, DAMPT at Cambridge Univ., had a chance to see the movie of this test. After watching the movie of the explosion, he calculated the energy of the explosion following his self-similar solution given in Eq. (10). Finally, he obtained that the explosion energy is about 20 kilo-ton TNT,[99] which was the number classified as top secret in the project.

5.3. *Non-LTE atomic processes in supernova remnants*

In the X-ray astronomy, the abundance of heavy elements (Si, Mg, Ca, Fe, etc.) ejected by supernova explosion is studied by use of the line emission from such heavy elements. A typical X-ray spectrum from SNR taken by Japanese satellite "ASCA" is shown in Fig. 15. Even at 10^3 years after the heating by the blast wave, the atoms are not in the thermodynamical equilibrium state, yet; and are still in ionizing phase. This is because the ionizing process by electron collision is extremely slow due to the low density of ISM. In addition, the ions are heated up by the shock wave, while the electrons are heated very slowly through the temperature relaxation process by Coulomb collision with the ions. As the result, the ion temperature is in general higher than the electron temperature inside the blast wave. Although, of course, there have been published papers insisting the anomalous effect on the ion-electron temperature relaxation, we limit our discussion to the Coulomb collision case.

In case of Coulomb collision, the temperature relaxation time as well as the collisional ionization time are proportional to the inverse of the electron density. They of course depend on the temperature in complex manner. The ionization stage of the inside of SNR is determined by the ionization parameter τ defined simply to be[100]

$$\tau = n_e t, \tag{11}$$

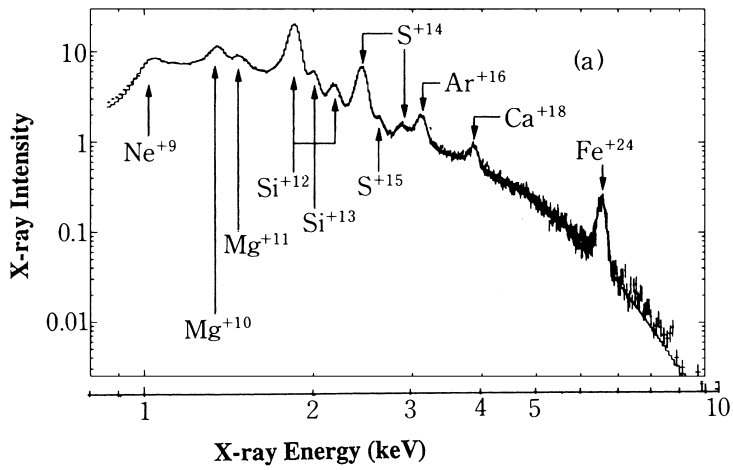

Fig. 15. A typical X-ray spectrum from SNRs observed by Japanese X-ray satellite "ASCA". The intensity of each line emission has information of heavy element nucleosynthesis in the progenitor of a supernova. The atoms in SNRs, however, are not in LTE and time dipendent non-LTE atomic physics becomes a key physics to connect the observed data to the nucleosynthesis scenario.

where n_e is the electron density and t is the age of the SNR. In the simulation of the atomic process with constant electron density ($n_e = 1$ cm^{-3}) and ion temperature ($T_i = 1$ keV), the electron temperature becomes comparable to the ion temperature at $\tau = 10^{11}$–10^{12} [s/cm^3]. At the same time the charge state of Si and Fe reaches almost to the thermodynamical equilibrium state.

In Fig. 14, the point crossing the line of the laser blast wave with the same temperature (same r/t) has the difference of time by a factor of 10^{19}. However, the density difference is the factor of 10^{18} and not completely coincides within the present simple discussion. It would be a good trial to scale down the blast wave in the universe into the laboratory from not only hydrodynamics point but also the point of atomic process.

There are, of course, many un-solved problem regarding non-LTE atomic process of SNRs.[100] The plasma inside SNRs is not only in LTE, but also ion-electron energy relaxation time is longer in some case than the age of SNR. For example, it is 10^4 years for the typical parameters; $n_e = 1$ cm^{-3} and $T_i = 1$ keV. Therefore, the electron temperature is probably much less than the ion temperature in most of young SNRs. In addition, the thermarization time of electrons, the time for electrons to become Maxwellian, is about 10^3 years. In the future when the observation technology advances substantially, we will have to discuss non-LTE atomic process of the plasmas with non-Maxwellian electron distribution. Actually, laser heated plasma is in general non-Maxwellian.[101] Since this affects the transport of electron very much as described in Appendix B, the non-local transport is solved with Fokker-Planck equation.[101] The non-Maxwellian distribution is measured experimentally when an ultra-intense laser is irradiated to ionize a solid foil.[102] The atomic process in the plasmas characterized with non-Maxwellian electron distribution is a hard job, while it will be required in the near future.

The same kind of discussion on the importance of the non-equilibrium ionization atomic process was pointed out relating to the X-ray observation of solar flare.[103] This is observed with Japanese solar X-ray satellite YOHKOH.[104] In the solar flares, the plasma temperature increases to a few keV in about 100 seconds.[105] The electron density is typically 10^{10} cm^{-3} and the ionization parameter becomes 10^{12} cm^{-3}s. With such value of the ionization parameter, the hydrogen-like and helium-like iron are expected in ionization equilibrium. However, the ion abundance derived from X-ray spectra from solar flare suggests the plasmas are not in ionization equilibrium. Therefore, in order to estimate time evolution of the plasma in solar flare, it is required to solve appropriate rate equation to iron and other spices including flows in solar flare. To verify such code would also be a good target for model experiment with intense lasers.

5.4. *Vishiniac instability*

In obtaining the self-similar solution of Taylor-Sedov blast wave, we have assumed it spherically symmetric. This can be confirmed by analyzing linear stability for the perturbations, namely a rippling of the front surface of the blast wave. It was carried out by assuming the density structure of the blast wave being in a thin shell form. After a complicated analysis, Vishinac[106] pointed out that the Taylor-Sedov

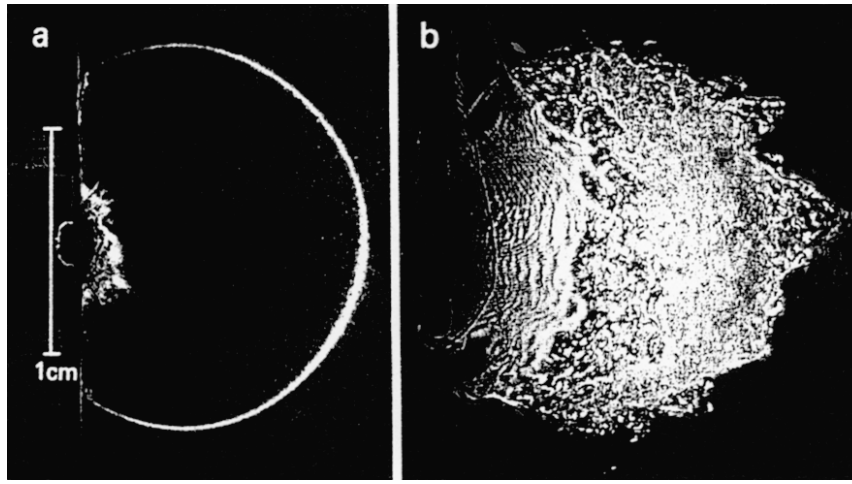

Fig. 16. Both are laser-produced blast waves. (a) is the case when laser is irradiated on the aluminum foil placed in the nitrogen gas, while (b) is the case when laser is irradiated on the aluminum foil placed in the xenon gas. In case with nitrogen gas, the blast wave is stable and estimated γ with Eqs. (10) and (13) was 1.3. On the other hand, in the case of the xenon gas, the xenon is ionized by the blast wave and cooled by the radiation emission. As the result, the effective γ reduces to 1.06, consequently unstable to Rayleigh-Taylor instability. Highly developed turbulent state was measured.

solution is unstable for the case with the specific heat ratio γ near unity. It is well known that the specific heat ratio is given in the following relation with the number of freedom of the gas, N:

$$\gamma = (N + 2)/N. \tag{12}$$

The decrease of the value γ means the increase of freedom. In Fig. 16, the shadow image of two laser-produced blast waves are shown.[7] In these blast waves, intense lasers are irradiated on aluminum targets located in the different kinds of gases. The left is the case where the gas is nitrogen and relatively low-Z, while the right is the case where the gas is replaced with xenon gas, which is relatively high-Z. Since the blast wave is so strong, the gases are ionized and emit radiation. In the case of nitrogen, this radiation loss is not so effective to cool down the temperature in the shock-heated gas region and consequently the effective γ does not change so much. In the case of xenon, on the other hand, radiation cooling decreases the temperature of the shocked gas region and reduce the effective γ less than the critical value with which the instability starts to grow. The effective γ has been evaluated experimentally in Ref. 7) by adjusting the observed front trajectory given by Eq. (10).

It should be noted that α in Eq. (10) is the function of γ and its approximate form is given, for example, in Ref. 107);

$$\alpha = \{[75(\gamma - 1)(\gamma + 1)^2]/[16\pi(3\gamma - 1)]\}^{1/5}. \tag{13}$$

In case of nitrogen gas, the effective $\gamma = 1.3$, while in case of the xenon gas $\gamma = 1.06$ was concluded.[7] In estimating the trajectory of the turbulent blast wave, the mean radius is used to obtain γ value from Eqs. (10) and (13). These values are reasonable

comparing to the result of Vishiniac that the critical γ is $\gamma = 1.2$ (see Fig. 1 in Vishiniac and Ryu [106]).

It is instructive to note that the number of freedom increases when some additional physics become important in a given parameter region. In this case, the internal energy increased by the shock compression is re-distributed including the energy escaping away as radiation. This corresponds to the increase of the freedom from the thermodynamical view.

It is also important to explain why the blast wave front becomes unstable with the decrease of the effective γ value. At first one has to know that the blast wave front is decelerating as easily seen in Eq. (10). This means the inertial force (effective gravity) works from the shock-compressed high-density side to the un-shocked low-density side. This tends to, in general, unstable to Rayleigh-Taylor instability. The existence of the flow across the front, however, affects whether the discontinuous surface is unstable or not. In the case without gravitational force, the general theory was published more than 50 years ago by L. D. Landau. [108] According to his result, the shock surface is always stable. Regarding the reason why stable, there is an intuitive explanation by considering the geometrical optics of the shock front trajectory.

In case when the adiabatic γ approaches to unity, the compressibility becomes important in physical mechanism if the rippled blast wave is stable or unstable. The density ratio at the strong blast wave front is given with the Rankin-Hugoniot relation in the form:

$$\rho_1/\rho_0 = (\gamma + 1)/(\gamma - 1), \tag{14}$$

where ρ_1/ρ_0 is the density ratio across the shock discontinuity. This is the reason why the radiation cooling causes a disruption of the spherically symmetric blast wave. The stability of the blast wave front is theoretically studied in Ref. 106). The conclusion is that the ripple of the front grows with oscillation in time for the case with $\gamma < 1.2$. In addition, the instability does not exponentially grow, but grows in the form proportional to the power of time, $t^{S(\ell)}$, where $S(\ell)$ is complex and depend on the spherical wave-number ℓ. J. Grun et al. [7] has applied this theory and concluded that in their experiments with xenon gas, $\gamma = 1.06$ and $\mathrm{Re}(S) = 0.7$ at the most unstable wave-number $\log(\ell) = 1.7$. Such instability at the blast wave front is called overstability or corrugate instability. As shown with ZEUS-2D code by Mac Low and Norman, [106] the oscillating growth of the front and density ripple of the blast wave saturate in the nonlinear phase and the oscillatory motion remains. The clear physical explanation of the mechanism of the overstability is given in Fig. 1 in Ref. 106). Saying in short, the surface ripple oscillates and grows by the unbalance of the Lamb pressure force at the front and the thermal pressure force at the rear of the front shell.

A detailed two-dimensional simulation has been carried out to study the same physics in the case of SNR. [109] It is well known that at the beginning of SNR, the blast wave is adiabatic and Taylor-Sedov is a good solution, while at the later stage when the radiation cooling time scale becomes comparable to the age of SNR, SNR is no longer adiabatic. Then, the thickness of the density at the shock front becomes

thin and the density ratio increases. The same kind of break up of the blast wave is demonstrated numerically in Ref. 109). It is noted that the evolutional scenario of SNRs is well explained in, for example, Ref. 94).

In the universe, another energy loss mechanism becomes also important. It is the energy loss by the ejection of high-energy-particles accelerated by, for example, Fermi statistical acceleration around the shock front of SNR. It is still open question on the physical mechanism of the origin of the cosmic rays. It is, however, most plausible that the cosmic rays with energy upto 10^{15} stem from the acceleration by SNRs. It is demonstrated by two-dimensional code how the spatial structure of the forward and backward shock waves and the contact surface based on the Chivallier's self-similar-solution [68] is affected by the decrease of γ due to the energy loss by the generation of the high-energy particles.

Before closing this subsection, I would like to note two points relating to magnetic field. As well recognized, the shock wave of SNR is so-called collision-less shock. [110] The thickness of the shock front is extremely shorter than the collisional mean-free-path. It is said that the thickness is of the order of ion Larmor radius. The average strength of the magnetic field in ISM is 3 μGauss. In addition, in order to accept the Fermi statistical acceleration model, the magnetic field should not be uniform, but in turbulent state. Many magnetic islands by the turbulence play a role of scattering body for high-energy particles. It is useful to point out that a model experiment of collisionless shock formation and Fermi acceleration with laser-produced blast wave has been proposed by P. Drake. [111] He mentioned that we can expect the formation of collision-less shock and 5–10 times bounces of protons in a gas-filled chamber with the diameter of 5 m.

The second is regarding model experiments done by B. Ripin et al. [112] In their experiment, a blast wave is produced as mentioned previously and observed the phenomena of its expansion in a strong magnetic field. [112] This is a model experiment to see the effect of magnetic field in SNR and at the same time, it is also a model experiment for the case when a nuclear bomb is exploded in the ionosphere. The same kind of experiment has been also carried out in the former Soviet. [113]

5.5. *Stellar jets*

Thanks to beautiful pictures taken by HST, the stellar jets are now very familiar to many people having interest in the universe. [114] It is said that in the scenario of the star formation, a baby star accompanies an accretion disk and a part of the accreted material is ejected through magnetic force toward bi-polar directions. This is an engine of the jet and the ejected jets propagate over extremely long distance keeping its thickness almost constant. The typical velocity of the stellar jet is hundreds km/s and the Mach number defined by the speed of jet divided by the sound speed of the jet plasma is usually 10–20. Such stellar jets are called Herbig-Haro jets after the names of discoverers and abbreviated as HH jets. It is reported recently that with VLBA radio interference observation system the smallest HH jet has been observed by measuring the maser emissions from the heated molecules by the bow shock of the jet front. [115]

The accretion disk cited in the above scenario is clearly seen in HH30 jet taken

by HST.[114] Many different structures are seen in Ref. 114), while all of them are characterized with the same morphology. Their morphology and kinematics have been studied mainly with numerical simulations, and some concluded that radiation cooling is necessary to maintain a high aspect ratio (length/thickness).[116),117)] The morphology of the jet is sensitive to several parameters; for example, jet Mach number, density ratio between jet and ISM, radiation-cooling parameter χ introduced in Ref. 117), and so on. According to a recent numerical simulation,[118)] the jet can propagate keeping high aspect ratio if not only the radiation cooling is effective, but also the pressure confinement by shocked-ISM plays important role. The latter is that when a jet propagates in ISM, the bow shock is generated and the pressure of ISM surrounding the jet increases so as to balance the pressure with the jet. This confinement effect is also essential to realize high aspect ratio jet.

Model experiments with Nova laser[119)] and Gekko XII laser[120)] have been carried out to study the importance of the radiation cooling in jet propagation. The same velocity as HH jets can be easily achieved by irradiating lasers with intensity about 10^{14}–10^{15} W/cm^2. The experimental condition is shown in Fig. 17.[119)] The target is a gold disk with a conical hole with an open angle of 120 degree. The interior of the conical section is irradiated by five Nova beams so that the conical surface is uniformly heated and plasma expands axially symmetric. The laser pulse width is 100 ps and total energy is about 1 kilo Joule. The expanded plasma stagnates at the central axis and the directed motion along the axis is formed to propagate outward like a jet. The self-emission of X-ray and back-lighted X-ray are measured. The jet

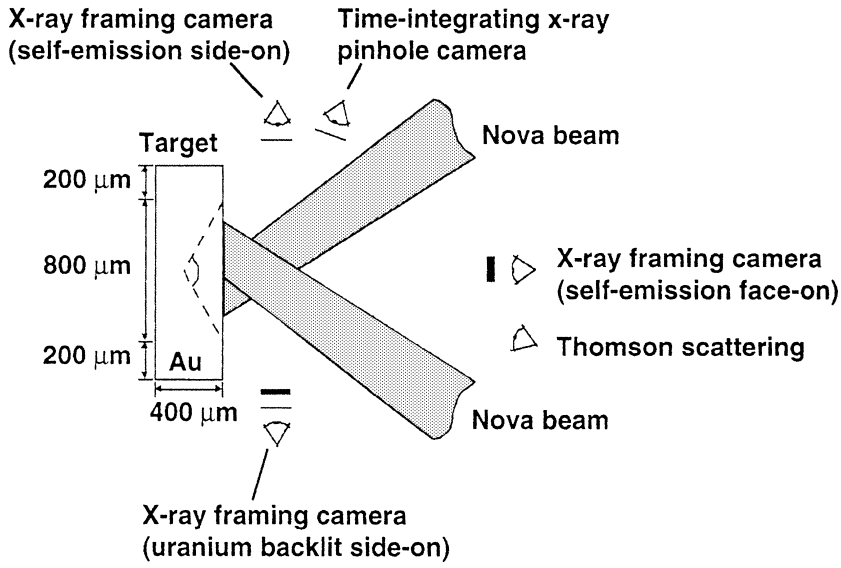

Fig. 17. Experimental arrangement of model experiment for stellar jet propagation. The target is a gold disk with a conical hole with an open angle of 120 degree. The inner surface of the conical section is irradiated by five laser beams so that the conical surface is uniformly heated and plasma expands in an axially symmetric way. Along with the collision of the plasma at the central axis, a jet is formed and the measured speed of the jet was 650 km/s.

speed of 650 km/s was observed and Mach number $M = 15$.[119] According to the astrophysical case,[117] the typical cooling parameter, which is defined to be

$$\chi = v_{\rm jet}\tau_{\rm rad}/r_0 = (\text{cooling length})/(\text{jet radius}), \tag{15}$$

where $v_{\rm jet}$ is the jet velocity, $\tau_{\rm rad}$ is the radiation cooling time and r_0 is the radius of the jet, takes the value $\chi = 0.1$–10. By the use of gold plasma, the cooling parameter $\chi = 1$ has been achieved in the experiment.

On the other hand, the second paper[120] describes more systematic study of the jet by varying the material of the target from low-Z plastic to high-Z gold. By varying the target, we can control the cooling parameter over the range of the astrophysical interest.

It should be noted that both experiments have been carried out in vacuum chamber and the shocked-ISM pressure confinement effect is not modeled. As the result, the jet-like structure once seen after the stagnation cannot propagate over relatively long distance and the jet disassembles finally as pointed out in Ref. 118).

These experiments are still premature. We have to study the effects of not only the ISM gas, but also the magnetic field. As clearly seen in HH47 picture by HST, the bow shock is formed at the front of the jet, and this is also collision-less shock in the background magnetic field. The effect of magnetic field should be studied by keeping, for example, the ratio of the dynamical pressure of jet (ρu^2) to the magnetic pressure. This topic resembles that of collision-less blast wave discussed in the previous subsection.

There are a variety of jets in the universe. One of the most exciting jets and the largest jet is the cosmological jet. The cosmological jet is composed of relativistic electron-positron plasmas and its scale is larger than galaxy. This jet could be modeled with ultra-intense lasers and will be described in the next section.

5.6. *Photo-ionized plasmas*

The photo excitation and ionization processes become important in a variety of astrophysical phenomena. As described in §4.4, the boundary forming the structure of the Eagle Nebula is the surface where the photo-ionization by UV radiation from nearby O/B stars is dominant and neutral hydrogen is ionized to be HII. Because of this, this region is called HII region.

In the present subsection, we only focus on the photo-ionized plasma near black hole or neutron star and consider a possibility of X-ray lasing (laser emission) in the universe. It is well known that maser from the universe is widely observed and has become a powerful tool for radio astronomy. The maser is coherent emission of microwave due to excited molecule. H_2O (water) maser and SiO masers are typical examples. The former mainly stems from the star-birth region,[121] while the latter is from star-death region.[122] Extremely huge scale water masers are also observed near the center of AGN (Active Galactic Nucleus) NGC4258.[123]

For X-ray astronomer, one of big dreams is to find a very strong line X-ray stemming from the inverse-population of atoms; namely to find X-ray laser in the universe. I briefly touch on the possibility in the plasmas photo-ionized by hard X-ray from the companion star.

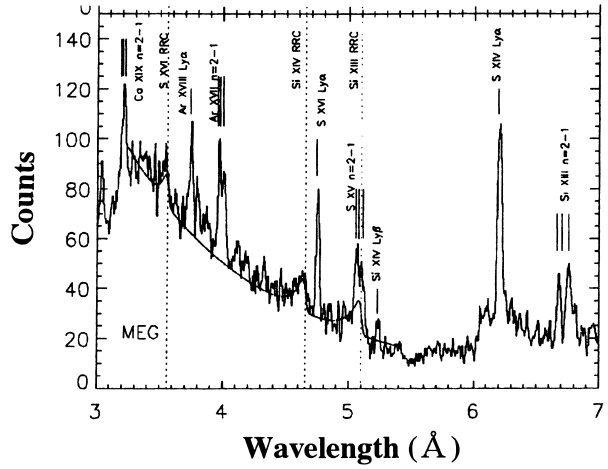

Fig. 18. X-ray spectrum of X-ray binary, Cygnus X-3, taken by US X-ray satellite "Chandra". Three radiative recombination continuums (RRCs) are used to determine the temperature of the free electrons. The solid, smooth line is a theoretical curve obtained by assuming the temperature of the free electrons 50 eV. The line emissions from highly charged Ca, Ar, S and Si indicate this cold plasma is photo-ionized by X-ray from the companion black hole or neutron star.

The group of Professor Kitamoto has observed X-ray spectrum from the third X-ray source in the Cygnus, Cygnus X-3, with Japanese X-ray satellite "ASCA". They have concluded that the X-ray spectrum comes from the atmosphere of a cold and relatively large star ionized by the X-ray emitted from the accretion disk of the companion black hole or neutron star.[124] It is well recognized that such compact binary emits strong X-ray, whose radiation temperature is in the range of keV.[125] In such a case, the companion star has strong stellar wind and is called Wolf-Rayet star. The stellar wind surrounds the companion star and the wind plasmas are ionized by the X-ray. According to Ref. 124), the plasma temperature is estimated from the width of RRC (Radiative Recombination Continuum) and the temperature of free electrons is estimated about 16 eV,[124] while observed X-ray spectrum shows strong line emission of H-like and He-like silicon, sulfur, etc. This is the direct evidence of photo-ionized plasma.

Recently, "Chandra" X-ray satellite of US has observed the same spectrum with higher resolution. A part of the spectrum is shown in Fig. 18.[126] The RRCs from SXVI, SiXIV and SXIII ions are fitted with a theoretical curve obtained by assuming the free electron temperature 50 eV. In Fig. 18, the theoretical curve is plotted with the solid curve relatively smooth and the edges of RRCs are indicated with the dotted lines. The concluded temperature is different from that with "ASCA", while it does not change the fact that the plasma temperature is low enough and the line emission from highly charged metal ions does not stem from thermally ionized ions. It can be concluded that the companion star of Cygnus X-3 is ionized by strong photons from the other compact companion star.

It is important to study the properties of the photo-ionized plasmas with some

model experiment with intense lasers. It is rather easy with gold cavity to make a radiation source whose radiation temperature is at highest 300 eV.[15] We can regard this radiation as that from black hole and irradiate on a low temperature plasma produced with another laser beam. By observing self-emission and transmitted X-ray from the cold plasma, we can study the photo-ionization process. In this case, the dimensionless parameter called ionization parameter ξ defined to be;[127]

$$\xi = L/nR^2, \tag{16}$$

should be kept same as the photo-ionized plasma in the universe. In Eq. (16), L is the luminosity of black hole or neutron star (total energy emitting per second) in the unit of [erg/s], R is the distance of plasma from the X-ray source [cm], and n is the electron density of the plasma [cm^{-3}]. In this model, a compact X-ray source is assumed to locate at the center and the cold plasma is at radius R. It is noted that L/R^2 is proportional to the X-ray intensity on the plasma surface.

Roughly speaking, the ionization stage of low-density plasma is controlled by the balance between the photo-ionization rate and radiative recombination rate. The former is proportional to the radiation intensity (L/R^2), while the latter is proportional to the electron density (n). A comprehensive study has been carried out in Ref. 128). It is well demonstrated that the ionization parameter ξ is a good parameter to measure the ionization stage of the photo-ionized plasma and most of medium-Z atoms such as neon, silicon sulfur and iron change from neutral ($\xi = 0.1$) to fully ionized ($\xi = 1000$).

Preliminary laser experiment has been carried out by keeping the ionization parameter constant.[129] According to a model calculation, it is demonstrated that the almost same charge distribution can be realized in both of low-density (10^3 cm^{-3}) and high-density (10^{20} cm^{-3}) cases.[129] We have tried to clarify the condition under which a stationary solution of the inverse population is realized around the present situation; however, we has not succeed yet.[130]

§6. Laser produced relativistic plasmas

As has been explained in relation to Fig. 1, the power of lasers has increased to PW (peta: 10^{15}) in the last ten years. This has become possible by use of CPA (chirped pulse amplification) technique.[14] It is well known that the solid amplifier like glass does not work when the laser intensity becomes more than GW/cm^2, because the optical properties of the glass are no longer linear above such laser intensity and, for example, nonlinear self-focusing tends to lead the optical damage. The CPA technique stretches the pulse width from fs- to ps-width before laser amplification by use of dispersion properties of grating reflector.[14] Then, the intensity can be reduced by 10^3–10^4 times lower. After the amplification of the longer pulse laser, the pulse is compressed in time with a large-scale grating reflector. This is just to do the reverse process done before amplification. By this pulse compression, we can obtain the laser output of 1–10 TW/cm^2. Increasing the final size of laser beam as 10^2–10^3 cm^2, we can realize PW laser system. By focusing PW laser on a target with a focused diameter of a few ten μm, we can obtain the laser intensity over 10^{20} W/cm^2.

It is useful to inform the reader that many institutions in the world constructed or now are under construction of such PW laser systems. For example, the pioneering construction was done at LLNL (Lawrence Livermore National Lab.) [131] and a variety of experiments have been done, a part of which I would like to explain from now. PW laser is under construction and almost completed at ILE, Osaka University. [132] France, UK and Germany are also constructing PW laser system for a variety of exotic subjects. In Japan, Kansai JAERI at Kizu in Kyoto constructed high repetition rate 100 TW laser system [133] and is constructing table-top PW laser. [134]

6.1. *Relativistic electron production*

When the laser light is irradiated on matter, a charged particle with charge q and mass m quivers in the electric field of laser with the quivering velocity $V_{\rm os}$ and its averaged kinetic energy $E_{\rm os}$ are calculated in non-relativistic case to be in the form;

$$E_{\rm os} = 1/2mV_{\rm os}^2, \quad V_{\rm os} = qE/m\omega, \tag{17}$$

where E is the amplitude of the electric field of laser and ω the laser frequency. In the case of electrons, the quivering velocity becomes the speed of light at the laser intensity $I_L = 3 \times 10^{18}$ W/cm^2 for typical glass laser, the wavelength of which is 1.06 μm. Roughly speaking, the laser energy is converted to those of high-energy electrons and their energies are about the quivering energy given in Eq. (17). This means, by use of PW laser we can produce substantially relativistic electron plasmas.

More general form of the electron quivering energy is given in the form:

$$E_{\rm os}^R = \gamma mc^2, \tag{18}$$

where c is the speed of light and γ is Lorentz factor of the quivering electron averaged over one cycle. This is calculated with the vector potential $A(= E/\omega)$ of laser to be

$$\gamma = (1 + a^2)^{1/2}, \quad a = eA/mc. \tag{19}$$

In Eq. (19), a is the normalized electric field and $a = V_{\rm os}/c$ is also satisfied. This means if a is of the order of unity, the kinetics is already relativistic. In case of $I_L = 10^{20}$ W/cm^2, $a = 6$ and $E_{\rm os}^R = 3$ MeV.

The ponderomotive force frequently cited in plasma physics, which is a nonlinear force due to electron quivering motion and roughly equivalent to the force by photon pressure, is given to be

$$F_{NL} = -mc^2\nabla(\gamma). \tag{20}$$

One of the high-energy electron production mechanisms is said that electrons are pushed forward like a ball of billiards and get energy of the potential difference given by Eq. (20). The photon pressure for the case of $I_L = 10^{20}$ W/cm^2 is 0.3 Tbar and this value is almost equivalent to that at the center of the sun (0.23 Tbar).

The acceleration mechanism of the high-energy electron is not unique, and if laser is focused on a low density plasmas, electrons with much higher energy are produced. This is easily understood by knowing that by controlling plasma wave or wake field by laser irradiation, strong gradient field like TeV/m is attempted to be produced. Such

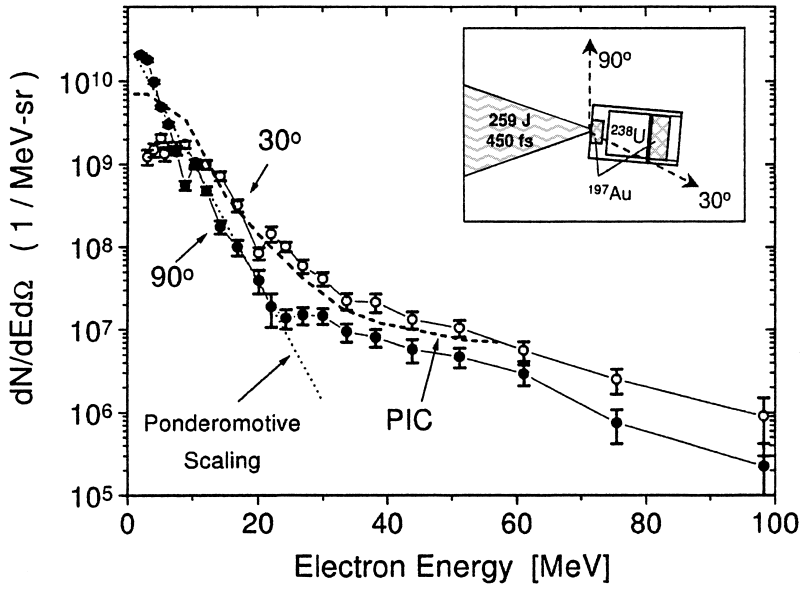

Fig. 19. Electron energy spectra measured in two directions as shown in the above box, when laser is irradiated on a gold foil with the intensity 6×10^{20} W/cm^2. The temperature of the bulk high-energy component is explained with ponderomotive scaling, while another substantial ultra-high-energy component is also seen upto 100 MeV. The corresponding particle-in-cell (PIC) simulation explains the experimental spectra.

study is called "laser acceleration" and has been studied for a quite long time.[135] In Rutherford Appleton Lab. in UK, for example, demonstrated particle acceleration upto 100 MeV.[136] In Fig. 19, the electron energy spectrum experimentally obtained when an ultra-intense laser is irradiated on solid gold at intensity of 10^{20} W/cm^2.[137] In Fig. 19, the dashed line with indication "ponderomotive" corresponds to the average energy in Eq. (18). It is clear that the physical mechanism intuitively explained above explain the high-energy electron of the bulk, while a substantial amount of high-energy electron with energy more than 20 MeV also exists. This component is thought to be due to the above laser acceleration mechanism. It is noted that the energy conversion rate from laser to such high-energy electrons is estimated 40 % in this experiment.

6.2. *A variety of physics triggered by relativistic electrons*

A variety of nuclear reactions and QED (quantum electro-dynamics) phenomena can be expected in the solid target being impinged by relativistic electrons. In the experiment, the target as shown right-top in Fig. 19 is used.[137] The target is made of ^{197}Au (0.3 g) and ^{238}U (1.2 g) layers cased with copper. The relativistic electrons do not directly interact with nuclei, but interact with the γ-ray produced by bremsstrahlung. The γ-ray with the energy of tens of MeV induces a variety of photo-nuclear reactions. Then, as shown schematically in Fig. 20,[138] some γ-rays activate gold nuclei and others triggers nuclear-fission of uranium. In addition, electron-positron pairs are produced through the interaction with field by gold nuclei.

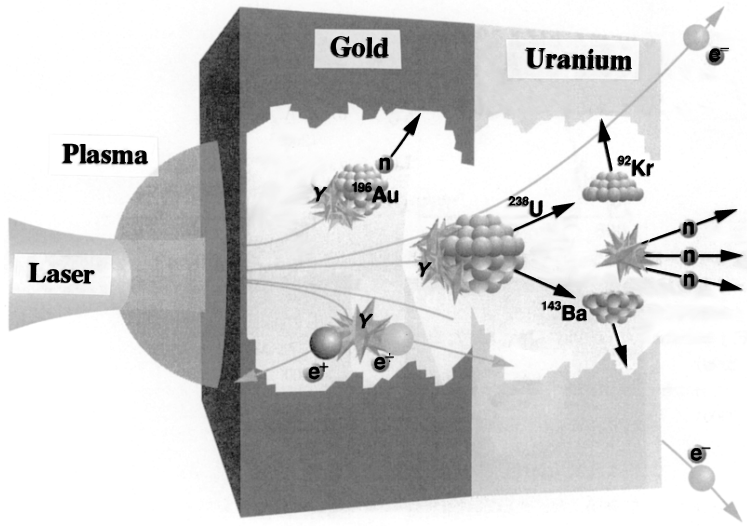

Fig. 20. Artistic picture on what happens when an ultra-intense laser is irradiated on a gold foil attached by uranium on the rear side. The generated high-energy electrons produce γ-rays, which consequently lead to pair creation, photo-nuclear activation, and photo-nuclear-fission.

At first, let us see the case of photo-activation of gold nuclei. For example, ^{197}Au (γ, xn) $^{197-x}$Au reactions take place for the energy of γ-ray more than 8.5 MeV. And, for example, ^{197}Au which lost one neutron ($x = 1$ case) decays to ^{196}Pt by β^+ decay process with emitting a hard X-ray of 356 keV. Such hard X-ray has been observed in the experiment.[137] At second, in the same experiment the photo-induced nuclear fission has also been observed. The structures of the fragmented elements well fit the theoretical structure.[137] This is described with the process ^{258}U (γ, f) and has the threshold energy of 5 Mev for the γ-ray. In the experiment the fission events of 1.8×10^7 were observed. This photo-induced nuclear reaction is not new itself. The possibility of such reaction was already pointed out by Bohr and Wheeler in 1939 in relation to the process inside stars. In addition, a variety of experiments have been done in 1970s with use of γ-ray produced by impinge of electron beams to matter. However, it is very new to have observed such reactions induced by ultra-intense lasers.

The third one is the positron production. The detail of this has been studied theoretically and compared to the experimental result.[139] I would like to describe this topics in the next subsection, because the electron-positron pair plasma may be used to model experiments for studying high-energy astrophysics.

6.3. *Positron creation by ultra-intense lasers*

The most direct process to induce pair production of electron and positron is through the vacuum polarization by the strong electric field of laser.[140] The threshold intensity to induce this "vacuum breakdown" is easily estimated by requiring the potential energy eE of the laser field over the distance of the electron Compton wavelength $\lambda_C [= h/(2\pi mc)]$ is equal to the total rest mass energy of the pair $2mc^2$. Then,

we obtain the following threshold laser intensity for the vacuum breakdown:

$$I_{VB} = \varepsilon_0 c E^2 = 5 \times 10^{28} \text{ W/cm}^2. \tag{21}$$

This intensity is too high at the present time to achieve technically. Therefore, it is more plausible to create positrons via high-energy electrons with the energy of tens of MeV.

In the present situation, there are mainly two processes to create electron-positron pair. They are

$$\text{(Trident process)} \qquad e^- + Z \to e^+ + 2e^- + Z, \tag{22}$$

$$\text{(Bethe-Heitler process)} \qquad e^- + Z \to \gamma + e^- + Z,$$
$$\gamma + Z' \to e^+ + e^- + Z'. \tag{23}$$

Trident process is a single process, while the Bethe-Heitler (BH) process is a two-stage process. In the BH process, namely, the electron energy is once converted to that of γ-ray and the γ-ray interacts with nuclei to create pairs. Which one contributes stronger to generate positrons in the present situation has been studied in Ref. 139).

The production of positrons has already pointed out in early time.[140] In Ref. 140), however, the author just estimated the threshold laser intensity over which pair production occurs owing to the Trident process and concluded that pairs are produced when the laser intensity is higher than 10^{19} W/cm^2.[140] Liang et al. considered the case when the high energy electrons are confined in a relatively thin gold foil and concluded that the Trident process is more important than the Bethe-Heitler process for the case of the foil with the thickness 1 μm.[141] On the other hand, Gryaznykh et al. have considered the case of relatively thick target and concluded that the BH process is more important.[142]

Such results can be guessed by the absolute values of the cross-section of these two processes. In Fig. 21, the energy dependence of the cross-sections of Trident process and the second stage of the Bethe-Heitler process is plotted. It is surprising that the cross-section of the Trident process is about by factor 100 smaller than that of the second process of the BH process. It is easily understood from this figure that if the energy conversion rate to γ-ray by bremsstrahlung from high-energy electrons is more than 1/100, Bethe-Heilter process becomes dominant compared to Trident process. This is the case of a relatively thick target. The physical reason is roughly explained as follows. In case of Trident process, the creation rate increases in proportion to the thickness of the shell. In the BH process, on the other hand, the number of the produced γ-ray increases in proportion to the thickness and in addition the number of interaction of the γ-ray increases in proportion to the foil thickness. Such difference of the dependency on the thickness stems from whether the process is single- or two-stage. Although the thickness with which both processes balance depends on the temperature of the high-energy electrons, the thickness is found to be 20 μm for the case with 4 MeV.[139] It is also informative to point out that the less value of the cross-section in Trident process seen in Fig. 21 is due to the fact that electron-nucleus interaction is in general via virtual photons with broad energy

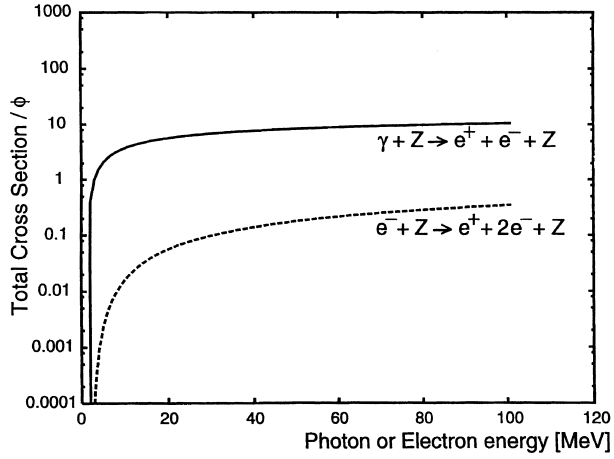

Fig. 21. The normalized reaction cross sections of the second stage of Bethe-Heitler process (solid line) and Trident process (dashed line). The normalization quantity ϕ is defined to be $\phi = (Z^2/137)r_e^2 = 0.58Z^2$ [milli-barn]. In case of nuclear reaction, an electron interacts with a nucleus through virtual photons, and in general the probability of interaction reduces about by a factor 100 in most of interactions.

spectrum. The same tendency can be seen in any cross-section of electron-nucleus interaction experiments with collimated high-energy electron beam.[143)]

Recently, we have calculated such pair creation issue by solving relativistic Fokker-Planck equations for the high-energy electrons and the created positrons by coupling with the γ-photon transport in the gold foil.[139)] The standard parameters for the numerical simulation are taken from the values of the experiment done at LLNL.[144)] We could obtain a good coincidence on the energy spectrum of the produced positron compared to that observed in the experiment.

6.4. *Model experiments with relativistic electron-positron plasmas*

The relativistic electron-positron plasma is an essential ingredient in high-energy astrophysics. In the high-energy astrophysics, for example, the active matter near black hole should be studied. In general, the temperature of the matter is extremely high because of the conversion of the gravitational energy to thermal energy in the accretion disk surrounding the black hole. Let us define a non-dimensional temperature $\theta = kT/mc^2$, where T is the temperature. In the thermodynamic equilibrium state, a large number of electron-positron pairs are created when the temperature approaches relativistic. If the density of baryon is low enough compared to, for example, a typical value at the center of stars, the positron density increases dramatically near relativistic temperature. For example, it is estimated 10^{25} cm^{-3} at $\theta = 0.1$.[145),146)] In such regime, the black body radiation has photons whose energy is higher than the rest mass energy of electron and the electon-positron pairs are produced by photon-photon collision. The electron-positron plasmas with photons are in the normal state in the range for $0.1 < \theta < 10$.[147)] If the temperature increases higher than this region, pion and muon plasmas ($\mu^+, \mu^-, \pi^+, \pi^-, \pi^0$, photon) becomes dominant. In most of the topics in high-energy astrophysics, the electron-positron

plasmas become an academic target to be studied.

The electron positron plasmas appear to be important in studying the plasmas over the surface of pulsars, those near black holes, those at the center of our galaxy, those at the active galactic nuclei (AGN), and those of MeV epoch in the Big Bang. Let us see the properties of such plasmas one by one.

At first, let us see the case of pair production over the surface of pulsar.[148] The pulsar has extremely strong magnetic field, ($\sim 10^{12}$ gauss) and is rotating with the rotation period in the range milli-second to second. In general, the poles of the rotation do not coincide with the poles of the magnetic-dipole. Due to the rotation, strong electric field is generated even though electrons are supplied to cancel this electric field. In such a strong electric field, electrons almost freezing the magnetic field are accelerated along the magnetic field. Owing to the curvature of the magnetic field line, the electrons emit γ-rays and the γ-rays interact with the magnetic field to create electron-positron pairs. This process occurs like cascade and it is said that if one electron creates 10^3 pairs through the cascade process, the observational data are well explained.[149] It is said that such pair plasmas are injected into the circumstellar matter to drive shock waves. The laser produced pair plasmas can be used to study the interaction physics of the relativistic pair plasma with normal matter.

The evidence for the existence of positrons near the center of our galaxy has been observed directly as annihilation line emission of γ-ray at 511 MeV.[150] In the annihilation, two γ-photons are created so as to conserve the momentum of a pair. The cross-section of the annihilation is very small and roughly given to be $\sigma = \pi r_0^2$, where $r_0 = \alpha a_B$ and α is the fine structure constant and a_B is the Bohr radius. From the observed intensity of the annihilation line, it is found that 10^{43} positrons are annihilating every second.[151] The anti-matter jet ejecting from the galactic center is also observed by VLA radio observation. The same kind of annihilation line emission has been observed in the solar flare, Crab pulsar, X-ray binary Cyg X-1, AGN and GRB (gamma-ray burst).[152]

The third topics is a possibility of electron-positron pair plasma in the accretion disk in X-ray binary.[153),154] The X-ray binary consists of a black hole or neutron star and a normal gas star as already explained in §5.6 in relation to X-ray laser in the universe. The envelope of the gas star accretes on to the surface of the compact star and the gravitational energy is converted to thermal energy. In general, the temperature of the ion is much higher than the electron in the accretion disk, while both temperatures are high enough so that a lot of positrons are produced. Some of the X-ray binaries have bi-polar jets with the velocity of about 90 % of the speed of light. Typical example is SS433.[153] The jet may consist of proton, electron and positron. To study the physical mechanism of the propagation of such quasi-relativistic jet in ISM could be one of model experiments with lasers. It is noted that the Cyg X-3 explained in §5.6 is also an X-ray binary, while the plasma are ejecting from the compact star in spherically symmetric form.[154]

The active galactic nuclei (AGNs) are classified to be the galactic nuclei of rather young galaxy and have the luminosity in the range $L = 10^5$–10^{14} L_0 ($L_0 = 3.8 \times 10^{26}$ W; the solar luminosity). The quasar is a kind of AGN with the luminosity more than 10^{12} L_0. The most-luminous AGNs have luminosity 1000 times higher than its

mother galaxy. AGNs have huge black holes at the center and their typical mass is, for example, 3.6×10^7 $M_\odot$ ($M_\odot$; the solar mass) for the case of NGC4258. There is a very famous observation with H_2O maser emission from the accretion disk of the galaxy center as already pointed out in §5.6.[155] The distance to NGC4258 has been measured precisely to be 7.2 ± 0.3 Mpc.[156] The radius of the nucleus is also observed with maser emission and is $0.13 \sim 0.26$ pc.

In the accretion disk of such huge massive black hole, gravitational potential energy is extremely high and the plasmas in the accretion disk become extremely high temperature. The temperature of protons becomes about 100 MeV and that of electrons a few 100 keV. The generation mechanism of positrons in AGN is rather easy to understand. The jets from AGNs are called AGN jets or cosmological jets. The jets have extremely high aspect ratio [= (jet length)/(jet diameter)]. A typical diameter of the jet is 10^{19} cm near the nucleus, while the length of the jet is, in the longest case, 100 times the size of its galaxy, a few Mpc (10^{25} cm). The closest ultra-luminous radio galaxy is Cygnus A and the detail of this AGN and AGN jet are given in Ref. 157). Recently, a clear image of X-ray observed with US Chandra X-ray satellite has been released.[158] Another famous AGN jet is M87, and the detail near the central core observed by Japanese space VLBI, Haruka, is shown on the cover page of Japanese journal very recently.[159] The most of AGN jets have the velocity more than 99 % of the speed of light and the typical value of relativistic $\Gamma(= 1/[1 - (v/c)^2]^{1/2})$ is equal to 10.

There is no direct observation to identify the kind of the plasmas forming the jets. Very recently, however, it is concluded with the polarization spectroscopy of radio wave from the quasar 3C279 that the plasmas of the jets consist of electron-positron pairs.[160] With more comprehensive method, at least five AGN jets have been identified to consist of the pair plasmas.[161]

With the laser produced relativistic pair plasmas, we wish to carry out some model experiments on the physical mechanism of the relativistic jet propagation. It is noted that Kelvin-Helmholz type instability is observed near the center of the galaxy NGC1275[162] and also the quasar 3C273.[159] Such morphology of the anti-matter relativistic jet is also a target of our model experiment.

In the early universe, the temperature dropped abruptly after the Big Bang. At the time when the temperature is in the range of MeV, the universe is filled with the electron-positron plasma. From the present baryon asymmetry, it can be estimated that the number of protons and neutrons was roughly 10^{-9} to 10^{-10} of the number of light particles (electrons, positrons, photons, neutrinos) in the MeV epoch that prevails up to times about 1 sec after the Big Bang.[163] This almost baryon-free plasma is interesting target to be studied in relation to the fire-ball described below regarding the γ-ray burst. In Ref. 163), it is pointed out that the such plasma allows a spatio-temporally localized stable soliton, to borrow a phrase from nonlinear optics. It can be rightfully called "light bullets" and these light bullets, being a source of concentrated mass and energy, may suffer gravitational instability. This could be a possible mechanism for the large scale structure formation in the early universe. To generate relatively high-density relativistic and baryon-free pair plasmas could be a good start to study the electromagnetic instability driven in such exotic plasmas.

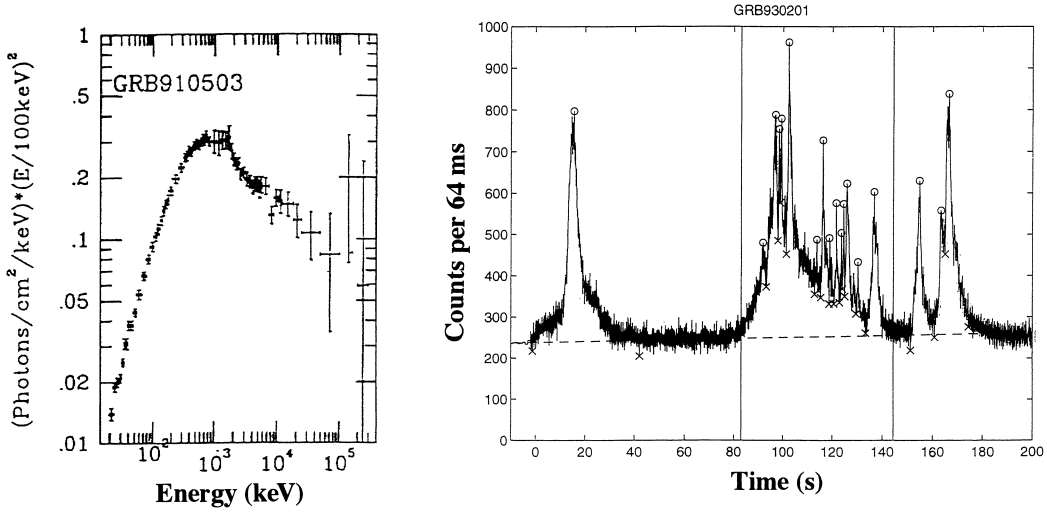

Fig. 22. A typical spectrum of GRB (left) and one example of time evolution of a GRB.

The gamma-ray burst (GRB) is the hottest academic target in the present astrophysics. The gamma-ray bursters are short-lived, extremely bright γ-ray sources. From the beginning of the accidental discovery in 1973 with the Vela satellites, whose main purpose was to ensure compliance with the 1963 Limited Test Ban Treaty of nuclear explosions, they have been attractive astrophysical enigmas.[164] The Italian-Dutch satellite BeppoSAX has identified that the γ-ray bursts are cosmological origin[165] and the estimated energy of each burst is about 10^{51-52} erg. In some case, it is estimated 3×10^{53} erg by assuming spherically uniform emission of the burst. It is more than 100 times larger than the energy of supernova explosion. The energy is extremely large and most of it is in the form of γ-ray and not X-ray nor visible light. The energy peak is in the range 100 keV to a few MeV. A variety of light curves of γ-ray have been observed and the duration of bursts is distributed from 0.1 to 100 seconds.[164] Examples of the GRB light curve (25–2000 keV) and the GRB spectrum are shown in Fig. 22.[164),166)] The light curves are not similar each other and six different types of light curve are shown in Ref. 164). GRB light curve shows rapid variability on time scales sometimes less than a millisecond. In one millisecond, light travels a distance $L = ct = 3 \times 10^7$ cm, which is about 10 neutron star radii. It is generally believed that GRBs originate from compact objects, such as neutron stars or black hole.[164]

The well-known model of the compact central engine of GRB is the so-called "fire-ball" model.[167] This assumes almost baryon-free energy source with the radius 10^{6-8} cm and energy 10^{51-52} erg. The mass fraction of the baryon should be fine-tuned in the range 10^{-2} to 10^{-3} in order to explain the observational data. This means most of the energy goes to photons, electrons and positrons. In the high-temperature limit in LTE, the fraction of the photon energy is 1/8 and the left 7/8 is in the form of energy of electron-positron plasmas.[145] The γ-rays are generated around the time when the fire-ball expands to the radius 10^{16} cm and the highly rel-

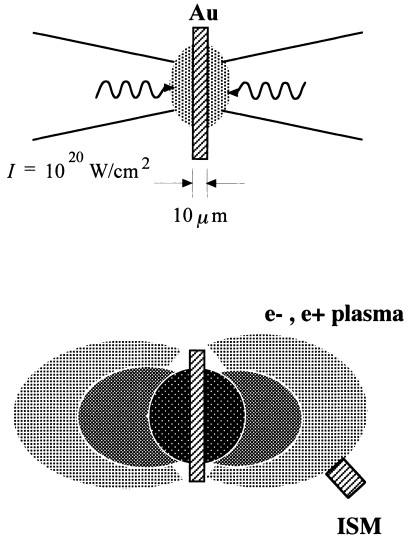

Fig. 23. A schematic picture of model experiment of a fireball of electron-positron plasma. Almost baryon-free pair plasma expands predominantly into vacuum.

ativistic baryon-shell or baryon-jet with the relativistic $\Gamma = 10^{2-3}$ is formed. During the expansion the fireball does not emit photons because it is optically thick and the energy of the fireball is converted to the kinetic energy of the baryon. The viability of the light curve in millisecond scale is explained, for example, by considering the collision of the baryon-shell or baryon-jet with clumpy and random ISM. More comprehensive explanation is given in Ref. 168).

In the last few years, the coincidence of the GRB and supernova has been observed.[169] "Hypernova" model has been proposed, where very massive star forms black hole at the center and the materials along the polar axis of rotation falls in hydrodynamical time-scale toward the central region because of no centrifugal force. Then, almost baryon-free two cones are produced in which the neutrino and anti-neutrino annihilation creates electron-positron plasmas. Detailed two-dimensional simulation of this "failed supernova" has been published[170] and the authors called this "Collapsars".

As same as above, GRBs require model experiments of relativistic electron-positron plasmas with small fraction of baryon. With intense lasers, we can generate very tiny baryon-free relativistic fireball in the laboratory. Un-avoidable difference is that the tiny fireball is optically thin, while the huge fireball in the universe is optically thick. We can see the properties of the fireball near the surface where the plasma is optically thin. The image of collision experiment of laser produced fireball with baryon (ISM) is shown in Fig. 23.

§7. Conclusion

I have reviewed my present understanding of possible model experiments of astrophysical phenomena with intense and ultra-intense lasers. It is described at

first that basic topics to be studied for laser fusion research can be divided to six topics. They are (1) Laser plasma interaction, (2) Electron energy transport, (3) Hydrodynamics and strong shocks, (4) Hydrodynamic instability, (5) Atomic physics and X-ray transport, and (6) Laser-produced relativistic plasmas, as shown in the vertical topic terms in Table I. The author proposed to introduce three views to consider and pick up model experiments suggested from each topic in laser fusion. They are (1) Sameness, (2) Similarity, and (3) Resemblance, as also shown in the horizontal topic terms in Table I. The matrix made of six rows and three columns gave us fifteen subjects of laser astrophysics at the present. The detailed explanation on astrophysical interest and possible model experiments for each topics has been given in the present paper. I hope this paper will motivate the readers to think and find a variety of new topics and the matrix table becomes black with many key words.

The model experiments of some of the topics have been carried out already. In contrast, some are not possible with the lasers available at the present time, but will be carried out in the near future with advancement of laser technology. The latter is mainly related to the experiments with ultra-intense lasers. In §6, I have explained just one experimental data obtained by Tom Cowan and his collaborators.[137),144)] It is, however, possible to increase the averaged energy of high-energy electrons by controlling the plasma density profiles to interact with lasers. For example, Pukov and Meyer-ter-Vehn have carried out three-dimensional particle simulation assuming the plasma with exponential density profile.[171)] They varied the laser power from TW to PW and corresponding intensity from 10^{18} W/cm^2 to 10^{21} W/cm^2. The resultant electron spectrum is given in Fig. 24. With the intensity 10^{21} W/cm^2 already achieved,[14)] for example, we can obtain the high-energy electron beam with average energy of 50 MeV by controlling the density profile. The authors emphasized that PW laser accelerates about 10^6 electrons up to 0.5 GeV energies on a distance as short as 30 μm, and this corresponds to an anomalous accelerating rate more than 10 TeV/m. They have obtained the scaling law of the temperature of the high energy electrons in the form;

$$T_{\rm eff} = \alpha I^{1/2}, \quad \alpha = 1.5 \text{ MeV}/(10^{18} \text{ W/cm}^2)^{1/2}. \tag{24}$$

It is noted that the resultant average energy of the high-energy electron is much higher than the case for solid target with sharp density profile, which was reported in Ref. 172). In addition, the scaling law of Eq. (24) depends on the density scale length.[173)] The present density scale length in the exponential profile is 30 μm. There have been published many papers on the acceleration mechanism up to such extremely high energy and it is not simple as intuitively explained in §6.1. Due to a strong ponderomotive force, for example, electrons are accelerated and extremely high current, which is much higher than the Alfven current limit $J_{\rm A} = mc^3\gamma/e = 17\gamma$ [kA], is produced. This current cannot be exactly compensated by the background electron return current. The strong quasi-static giga-gauss magnetic fields are generated leading to focusing or filamenting the electron flow. The electron acceleration mechanism, for example, by such magnetic field assist (MFA) mechanism has been studied.[174)]

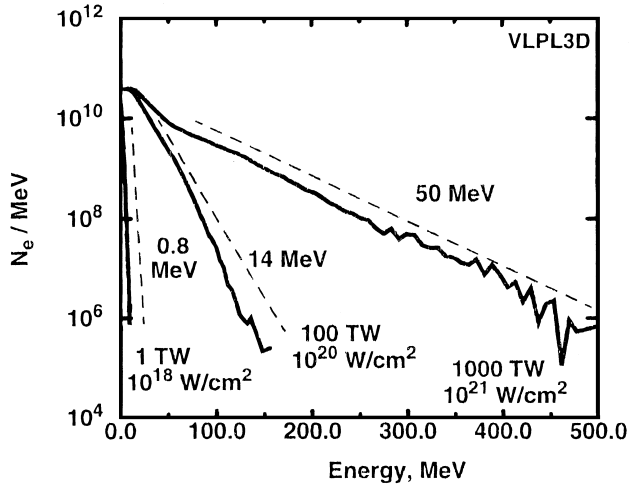

Fig. 24. Three-dimensional simulation results of high-energy electrons obtained when TW to PW lasers are irradiated on a plasma whose density profile is exponential with the scale-length 30 μm.

Experimental evidence of not only the high-energy electrons but also very energetic proton beam production has been also reported recently.[175] The energy distribution shows an effective temperature of about 5 MeV, with the most energetic ions around 50 MeV. The detailed particle simulation to explain the acceleration mechanism is also attempted.[176] It is well-accepted that such high energy protons are produced by the ambipolar field produced by the expanding high energy electron cloud on the rear surface of the target foil. Since the thickness of the cloud is much thinner than the focal spot size, the ambipolar filed is generated almost perpendicular to the rear surface of the target at each local point. By using a curved foil, therefore, we can focus the proton beam. This focusing has been demonstrated experimentally[177] and numerically with Vlasov-Maxwell solver.[178] In near future, it may be possible to construct a compact GeV positron source and G. Mourou,[179] for example, proposed to use this proton accelerator to generate neutrinos. Probably, we can design a variety of dream with the help of advancement of laser technology.

As mentioned above, designing the density profile of plasma we can increase the energy of the relativistic electrons even with the same laser intensity. Such study is important, for example, to design high-energy astrophysics model experiments. One issue is how to increase the number of positrons and to produce a bigger and denser electron-positron plasmas. In addition, the increase of the energy of the relativistic plasmas leads us to study a variety of nuclear physics. In Fig. 25, the result of "GEANT" code calculation is shown for the case when the high energy electrons given in Fig. 24 impinge in a tungsten foil. The figure shows all products at 8 mm from the surface of the tungsten foil.[180] The "GEANT" code has been developed at CERN for a long time under international collaboration.[181] It includes "EGGS" program in which a variety of nuclear reaction cross-sections are tabulated. In Fig. 25, the primary electron spectrum given by Ref. 171), the energy distribu-

tion of γ-ray by bremsstrahlung, and electron and positron distribution after 8 mm tungsten foil are shown. In addition, a still relevant production of several thousand pions per shot is sketched in the lowest curves. The right of Fig. 25 shows the cross section for photo-pion production via the $\Delta(1232)$-spinflip resonance of the nucleon at an energy of 294 MeV. Due to kinematics, the resonance is shifted to 310 MeV in the laboratory frame.

The high-energy astrophysics is strongly related to nuclear physics and elementary particle physics. Our laser astrophysics also directs these directions, and not only astrophysics, but also a new field in nuclear physics may be possibly born with revolutionary progress of laser technology.[182)]

I want to close this section by discussing a possibility to do some model experiment relating to general relativity and black holes. According to Einstein's "principle of equivalence",[183)] the properties of the motion in a non-inertial system are the same as those in an inertial system in the presence of a gravitational field. In other words, a non-inertial reference system is equivalent to a certain gravitational field. Let us simply estimate the acceleration in case of target implosion in laser fusion. The typical value of the past implosion experiments, the flight distance 200 μm over 1 ns,[59)] gives us the acceleration 10^{13} G, where G is the gravity on the earth.

By use of ultra-intense lasers, we can accelerate a thin foil about 10 μm over 1 ps. The average acceleration is about 10^{18} G. For example, the strong gravitational field on the surface of a neutron star with a solar mass (2×10^{33} g) and 10 km in radius is calculated to be about 10^{11} G. It was observed that a strong red-shift of iron K-α absorption line in the X-ray spectrum coming from the surface of a neutron star.[184)] We may be able to expect a red-shift of a line emission from an atom being accelerated by intense laser. However, this is not a general relativistic effect, because the photon does not feel any acceleration at the moment of emission. If the observer

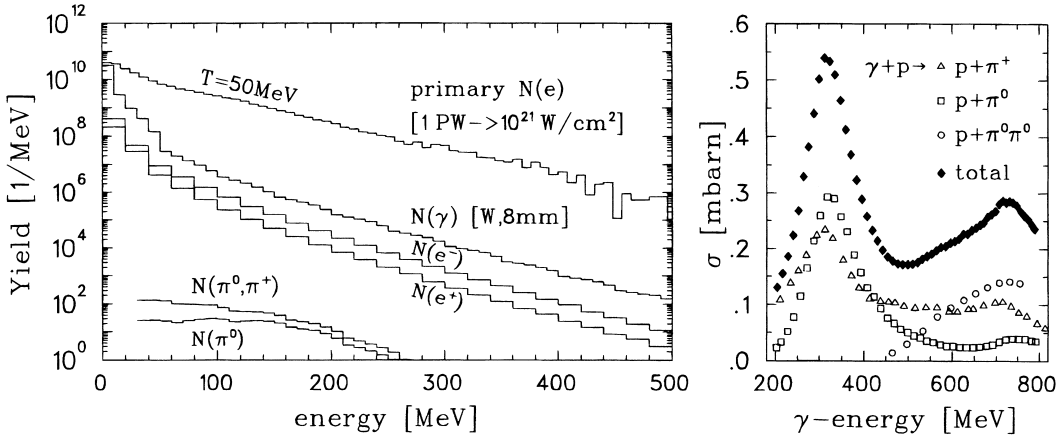

Fig. 25. The primary electron spectrum given in Fig. 24 with 50 MeV temperature, the energy distribution of γ-ray by bremsstrahlung, and electron and positron distribution after 8 mm tungsten foil are shown. The "GEANT" code is used for calculation. A relevant production of several thousand pions per shot is also calculated as shown in the lowest curves. The right figure indicates the cross section of pion production reaction when the γ-ray interact with proton.

is in the perpendicular direction to the accelerating atom, some red-shift will be observed and can be explained as perpendicular Doppler shift within the special relativity. We need more idea to direct evidence experiment of the general relativity and relate such model to experiment, for example, to probe the direct evidence of black holes.[185] It is also noted that the red-shift of line emission from a surface of a compact object is due to the deformation of the space. This cannot be realized even with ultra-intense lasers giving the acceleration stronger than the gravity of the compact object.

Finally, I would like to answer the question why I promote the astrophysics with lasers. In my career over 20 years in laser fusion research, many things have happened not only in the world of science, but also in the real world. The biggest would be the cease of Cold War.[186] Fusion research itself could not be independent of the political confronting in Cold War. After such dramatic change in the history, what I finally found was expressed with the words by Professor H. Yukawa.[187] That is, "I am a traveler ("Tabibito" in Japanese) without map". The fusion research is not engineering, but still many scientific issues have to be studied to draw the road map to the final goal, the production of fusion energy with realistic cost. The fusion energy research itself is a long range research and needs a variety of young talents to overcome the present and the future coming scientific obstacles. Someone says that "laser astrophysics is aiming at different direction and you have to keep your feet on the road to fusion energy". Is it correct comment to me? I believe what is required for fusion research is to support the fundamental research such as laser astrophysics to spread the academic standing field of fusion research. It could be the global standard in the 21st century to promote a big science with obtaining the understanding and support by many societies. The laser astrophysics is not only very attractive as an unique field of astrophysics but also important for fusion research to keep inter-disciplinary activity to export and import of rapidly growing achievements in each academic field.

Acknowledgements

The author would like to express his sincerely thanks to Professor F. Takahara for inviting me as lecturer of the Yukawa Memorial symposium and giving me a chance to review the laser astrophysics. He also thanks Dr. B. Remington at LLNL for his encouragement to promote this new field together. He also thanks Professor K. Nomoto who gave me a chance to get into the astrophysics through collaboration and for supporting the promotion of this new field. He also thanks Professor S. Yamada and the author's students for valuable discussions and indirect encouragements.

Appendix A

—— Physics Scenario of Laser Fusion ——

Schematic of laser fusion scenario is shown in Fig. A-1. Lasers are irradiated on a spherical target surface and an extremely high pressure is generated over the target surface. Then, strong shock waves accelerate the fuel toward the target center

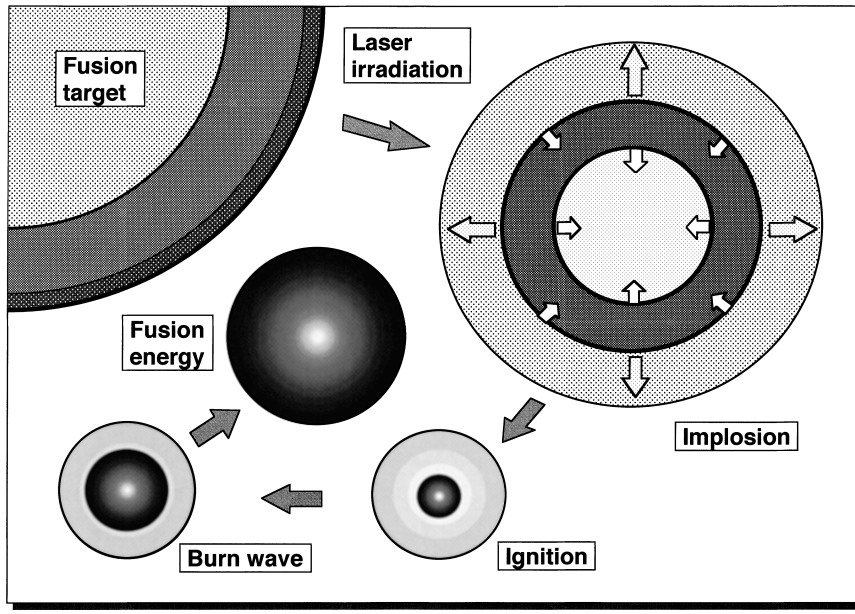

Fig. A-1. A schematic picture of spherically symmetric laser fusion scenario. In fusion reactors, a frozen deuterium-tritium fuel layered inside a plastic shell whose diameter is about 0.5 mm will be irradiated by many laser beams with total energy about 4 mega-Joule. Then, the surface material ablates and expands into vacuum and its reaction drives strong shock waves going toward the center of the target. This process is called "implosion". After the implosion, the central part of the fuel reaches the fusion ignition condition of temperature 5 keV and density over a thousand times the solid DT density (200 g/cm^3). If the compressed core size is larger than the stopping length of the alpha-particle, the self-heating occurs in an extremely short time and the nuclear burning wave is formed. Since the typical velocity of the burning wave, which is so-called nuclear detonation wave, is one order of magnitude higher than the velocity of the disassemble of the compressed fuel, the burning wave triggers the fusion reaction of the left fuel.

and finally compress the fuel more than 10^3 times the solid density. If the implosion is spherical enough and the central spark is large enough, the spark region ignites and the self-heating by produced alpha-particles leads to a generation of a fusion burning wave. Then, the main fuel compressed to surround the spark with as less entropy as possible is heated and burned to produce fusion energy more than 100 times the laser energy. This is a simple scenario of laser fusion. However, there are many physics issues to be studied in order to realize this scenario in a laboratory.

The physics scenario of the laser fusion proceeds from the top to bottom in Fig. A-2. The central flow represents the success scenario described above. The right-hand side represents the pre-heating due to supra-thermal electrons or X-rays, while the left-hand side concerns the physics related to the deformation from spherically symmetric implosion. The theoretical research issues in Fig. A-2 can be roughly divided into the following six. We briefly describe the summary of the present status of each subject.

(1) **Laser Plasma Interaction** has attracted many scientists regarding nonlinear

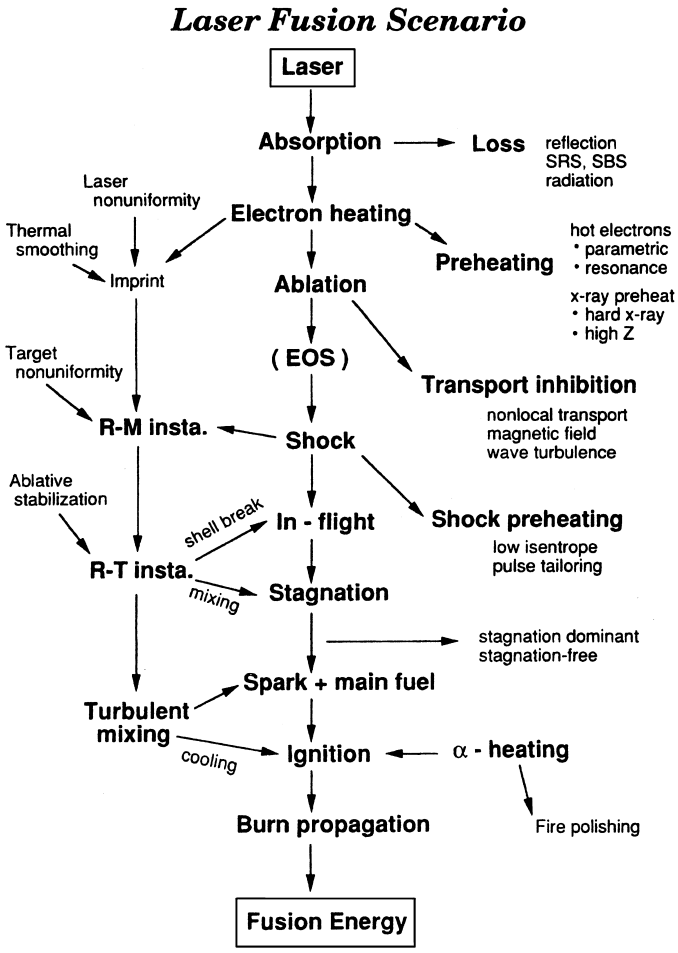

Fig. A-2. Flow chart of laser fusion physics scenario. The central flow is a success scenario within spherically symmetric and classical hydrodynamic physics. The absorbed laser energy is transported by electrons toward over-dense region and ablates the target surface and drives ablation pressure. The ablation pressure of several tens Mbar drives strong shock waves to accelerate the target toward the center. In the final compression phase, the accelerated fuel stagnates at the center to trigger fusion reaction and the alpha-particles, the fusion-reaction particles, burn most of fuel to produce the fusion energy more than 100 times the laser energy. The nature is, however, neither so simple nor so kind. Multi-dimensional effect whose physics scenario is shown on the left side should be avoided or controlled. In addition, non-classical transport whose physics scenario is shown on the right should be suppressed or, in some case, used to realize the main success scenario.

plasma physics such as parametric instabilities.[17] The peak of research was about 25 years ago. The transport of the supra-thermal electrons generated through the resonance absorption has been studied intensively about 20 years ago. As the results, physics modeling has already been established. However, this topics has revived recently in relation to the fast ignition scheme, which became principally possible after the invention of CPA technique. In this case, nonlinear physics of laser-plasma interaction should be studied in the relativistic regime, where the quivering energy of

a free electron due to laser field is comparable to or more than its rest mass energy. In addition, filamentation, self-focusing, magnetic field generation and so on should be studied.[174),188)]

(2) **Electron Energy Transport** is mainly focused on the kinetic effect of electrons; namely, non-Maxwell effect through laser heating and electron transport processes. Non-local heating by the tail component of electron distribution function should be studied based on Fokker-Planck type equation. This topics had been studied intensively about 20 years ago mainly in one-dimensional case. It is now in progress to install the Fokker-Planck solver in multi-dimensional hydrodynamic codes.[101)] Some hybrid schemes of kinetic and fluid descriptions of electrons are required to be modeled. In the fast ignition, strong magnetic fields in the range of 100 Mega gauss are generated and the electrons strongly couple with the magnetic fields.[174),188)] A new frontier of plasma physics is being opened.

(3) **Hydrodynamics and Strong Shocks** are based on the compressible hydrodynamics. The rocket model and coupling efficiency are well understood theoretically and have been checked by laser model experiments. The implosion experiments have been carried out in big institutes with multi-beam laser systems, and high temperature and high density compression has been achieved. What we have learnt, however, is that hydrodynamic mixing is the most critical issue and the fusion performance in the experiments is worse compared to the corresponding one-dimensional (1-D) simulations. Prescriptions to model the mixing in the codes have been developed and some are well improved to explain the experimental results.[189)] The prescriptions are potentially applicable to astrophysics problems, and the simple mixing length theory would be replaced with them.

(4) **Hydrodynamic Instability** is the main of laser fusion physics. It is just simple to generate fusion energy, if the nature is kind enough to allow the implosion to be spherically symmetric. It is, however, natural to see hydrodynamic instabilities in many cases. A light of hope is found to shine in the dark. This is called "ablative stabilization". There is a hope to be able to control the growth of Rayleigh-Taylor instability in the ablative acceleration phase. This was predicted theoretically more than a decade ago,[84)] and was experimentally confirmed recently in several institutes independently.[85)] Based on the accomplishment of physics in laser plasmas, theoretical works and model experiments are now opening new fields in the physics of compressible turbulent mixing.[190)] This is related to, of course, the astrophysics. Main concern is the physics of hydrodynamic instability driven by strong shock waves and pressures caused by energy transports due to not only charged particles but also radiation.

(5) **Atomic Process and X-ray Radiation Transport** require broad knowledge concerning atoms with multi-electrons, non-LTE atomic process, rate equations, database of rate coefficients, just to name a few. We also have to choose one from a variety of modeling; for example, average atom model or detailed configuration accounting. We are also required to develop or use sophisticated codes to calculate atomic structures and solve the rate equation. An organized promotion of research is required with involvement of many scientists. When medium or high Z material is used as a part of targets, radiation-hydrodynamics (RHD) becomes im-

portant. Coupling between the radiation and fluid is through opacity and emissivity of matters. Spectral opacity is very complex in partially ionized medium and high Z plasmas. The international opacity workshop has been held with attendance of more than 20 groups modeling opacities of hot-dense plasmas.[86] For example, UTA (unresolved transition array)[191] and STA (super transition array)[192),193] should be modeled for calculating the opacity of complex atoms in laser plasmas. In addition, non-LTE atomic process and ion population should be modeled by coupling with the hydrodynamic simulation codes. Very stiff computational task is required.

(6) **Laser Produced Relativistic Plasmas** are an attractive topics, especially in relation to astrophysics. With invention of chirped pulse amplification technique, we can achieve PW with the present technology. When the focused laser is irradiated on a foil or pre-formed plasmas, the quivering energy of electron exceeds the rest mass energy and all phenomena become relativistic. Such relativistic electrons generate γ-rays and the γ-rays interact with nuclei to activate nuclei, trigger photo-nuclear reactions, and generate electron-positron pairs. Regarding the fast ignition scheme, the scaling law of the averaged energy of the relativistic electrons and energy conversion rate from laser energy to the relativistic electrons are important to be studied systematically. In addition, the transport of the relativistic electrons and generation of energetic protons are also related to designing the core ignition by the fast ignition scheme.

Appendix B

Laser Plasma Interaction and Electron Transport

When an intense laser is irradiated on a solid material, the very strong electric field of the laser breaks down the material and free electrons are generated. The free electrons are quivered by the laser field to ionized and increase the number of free electrons. When the material is almost ionized, the free electrons obtain more energy through the inverse-bremsstrahlung process. Since the laser cannot penetrate over the critical density at which the laser frequency is equal to the plasma frequency, the laser coming from the vacuum penetrates into the plasma expanding into vacuum and reflected at the critical density region toward the vacuum direction. The absorption rate of the laser through such path is given by integrating the local absorption coefficient given to be

$$K_{\rm abs} = \nu_{ei}(\omega_{pe}/\omega)^2 V_g^{-1}, \tag{B·1}$$

where ω and ω_{pe} are the laser and plasma frequency. In Eq. (B·1), V_g is the group velocity of the laser and ν_{ei} is the Coulomb collision frequency of electron by the ion with charge Z. They are given in the forms:

$$V_g = c(1 - \omega_{pe}^2/\omega^2)^{1/2}, \tag{B·2}$$

$$\nu_{ei} = 3 \times 10^{-6} \ln \Lambda n_e Z / T_{\rm eV}^{3/2} [s^{-1}]. \tag{B·3}$$

In Eq. (B·2), $\ln \Lambda$ is the Coulomb logarithm and $T_{\rm eV}$ and n_e are the electron temperature in eV unit and the electron density in $\rm cm^{-3}$ unit of free electrons. It is clear

from Eq. (B·2) that the absorption rate is inversely proportional to the electron temperature.

The above formula is simply derived by assuming Maxwellian distribution for electrons. It is, however, pointed out that the electron distribution function of the laser-heated region is not Maxwellian, but flat-topped distribution appears. This is easily understood. From a microscopic view, the electron with low energy more frequently collides with ions than the electrons with high energy. Therefore, as laser heating goes on, the low energy component becomes less. This is called Langdon effect [194] and becomes important by coupling with the electron energy transport. [195]

In case where the laser intensity becomes high, the electron temperature increases so that the collisional absorption is not effective and another absorption process appears to be dominant. One is the resonance absorption. This depends on the incident angle of laser and the direction of laser field polarization. When the laser is obliquely incident to the equi-density surface, the density of the laser turning point is lower than the critical density. Due to the tunneling effect of wave, the electric field penetrates over the turning point and reach at the critical density surface. If the laser polarization is such that the electric field at the critical density is in the same direction as the density gradient, the charge separation is resonantly driven and the laser field energy is converted to the plasma wave energy. Finally the plasma wave losses its energy to thermal energy of electron through wave-particle interaction. This is also absorption, while most of energy is used to generate high-energy electrons. More details are given in, for example, Ref. 17).

Laser intensity is so high and the ponderomotive force, which is roughly equivalent to the force by photon pressure, plays a variety of role in laser-plasma interaction physics. Typical example is the parametric instabilities. These instabilities have been studied very intensively in 1970s and provided good examples of nonlinear plasma physics. I also suggest readers who wish to know more to read Ref. 17).

Finally, I would like to point out that the laser-plasma interaction physics becomes a very hot topics again recently after appearance of the ultra-intense lasers. In this case, however, the knowledge accumulated in 1970s cannot be directly applied, because relativistic effect of electrons plays essential role in these physics.

In laser fusion, the absorbed laser energy is converted to the thermal energy of electrons. Since the mean free path of the electrons is proportional to fourth power of the velocity, the high energy electrons penetrate over a long distance almost without collision. In the classical case, the diffusion type of the electron heat flux given by L. Spitzer is usually used. [196] This formulation is well described in Ref. 197). In the case when the temperature scale length becomes even shorter than 100 times the averaged mean free path, the Spitzer's formulation breaks and we have to solve Fokker-Planck equations for electron directly. [198),199] So high criterion of 100 times is due to the fact that the most of the heat flux is carried by the electrons whose velocity is 3.4 $v_{\rm th}$, where $v_{\rm th}$ is the thermal velocity of the electrons with Maxwellian distribution. In Fokker-Planck calculations, we get in general the following view of the electron distribution from laser heated region to ablation front. In the laser-heating region, due to Langdon effect, flattened Maxwellian distribution is seen, while near the ablation front the distribution function has enhanced

tail component coming freely from the laser-heated region. Such transport is called "non-local transport" and electron preheating over the ablation front occurs. For the convenience in installing such non-local transport model in an implosion code, an integral representation of the heat flux is also proposed.[200)]

It is time consuming to solve Fokker-Planck equation directly and carry out even one-dimensional implosion simulation.[201)] A hybrid type code in which the tail component is solved directly with FP equation, while the bulk component is solved with fluid description is under development in order to be coupled with one and two dimensional implosion codes.[202)]

It was reported that the non-local heating affects the growth of the Rayleigh-Taylor instability at the ablation front.[29)] However, many physics seem to appear in the vicinity of the ablation front and we did not come to the final conclusion yet on if the non-local transport is essential to RT growth at the ablation front.[46)] Kinetic treatment of electron with Fokker-Planck type equation is also required to study the electron transport in ultra-short pulse irradiation[203)] and essential to study QED issues in relativistic regime.[139)]

Appendix C

—— *Vortex Formation by Shock-Matter Interaction* ——

In the universe, interstellar shock waves play important role to heat up ISM. Since the topics related to the hydrodynamic instability and shock wave is one of the core of the laboratory astrophysics research with intense lasers, we briefly consider the physical mechanism of the shock-wave driven hydrodynamic instability such as Richitmyer-Meshkov (RM) instability. When a shock wave passes the region with density varying in space (e.g., a contact surface of different materials), velocity perturbations are generated to finally deform the structure of the contact surface. A perturbed contact surface is always unstable to this R-M instability regardless the shock wave passes from high density to low density or vice versa. The physical mechanism of R-M instability can be understood easily as follows.[5)]

The equation of motion of in-viscid fluid with the density ρ, flow velocity $\boldsymbol{u}$, and pressure P is given in the form;

$$d\boldsymbol{u}/dt = -\rho^{-1}\nabla P. \tag{C·1}$$

By taking the rotation of Eq. (C·1) and introducing the velocity defined to be

$$\omega = \nabla \times \boldsymbol{u}, \tag{C·2}$$

we can obtain the equation for the velocity

$$\frac{d\omega}{dt} = (\omega\nabla)\boldsymbol{u} - \omega(\nabla\boldsymbol{u}) + \frac{1}{\rho^2}\nabla\rho \times \nabla P. \tag{C·3}$$

In Eq. (C·3), the first term on the right-hand side (RHS) represents a force to stretch the three-dimensional vortex in the direction of the vector ω. This is the source term causing the cascade in the power spectrum of uniform turbulence in

three-dimension. The second term on RHS is proportional to div($\boldsymbol{u}$) and governs the effect of compressibility. This means that the vorticity is also compressed or expanded according to the compression or expansion of the fluid, respectively. The third term is called "baroclinic term" and becomes a source to generate the vortices, provided that the gradients of the density and the pressure are not in parallel.

When a shock wave (s.w.) comes from the left as shown in the top of Fig. A-3, the pressure gradient due to the shock wave is for the left as indicated in the circle in Fig. A-3. Let us then assume that the shock wave collides with the contact surface which separates a fluid with the density ρ_1 on the left and a fluid with the density of ρ_2 on the right. In addition, assume that the contact surface is not in parallel with the shock surface. The direction of the density gradient is opposite depending on whether ρ is lower (Case-A) or higher (Case-B) than ρ_2 as shown in the stretched view in Fig. A-3. It is obvious from the third term in Eq. (C·3) that in Case-A the vortices with the rotation in the clock-wise direction is generated at the contact surface, while in Case-B the direction of the rotation is in the counter direction. This is shown in the stretched view in Fig. A-3.

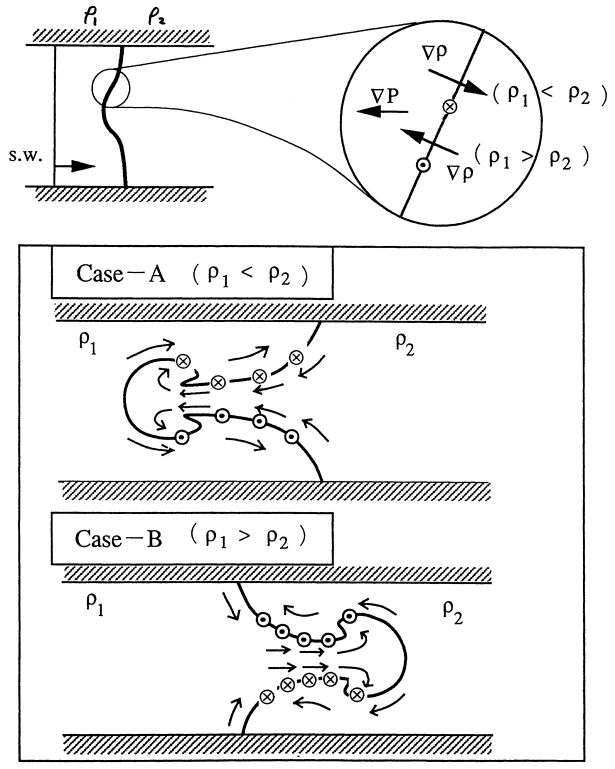

Fig. A-3. The physical mechanism of vortex formation by shock wave. As given in Eq. (C·3), vortices are generated when the pressure gradient of a shock wave is not in parallel to the density gradient. After the passage of the shock wave, the generated vortices at deformed contact surface induce further deformation of the contact surface. The flow field inducing the deformation can be guessed by use of the analogy of Eqs. (C·2) and (C·4). This gives an intuitive explanation of physics of Richtmyer-Meshkov instability as shown in Cases A and B in the figure.

When vortices are generated, fluid flow is generated to surround the vortices and the resultant fluid flow causes the deformation of the contact surface. For the initial perturbation given in Fig. A-3, two vortex sheets with opposite signs are formed in the upper and lower halves after the passage of the shock wave. It is easy to image the deformation by using the analogy of the relation between the electric current and magnetic field. When the current density $\boldsymbol{j}$ is given, the profile of the magnetic field $\boldsymbol{H}$ is obtained from the relation;

$$\nabla \times \boldsymbol{H} = \boldsymbol{j}. \qquad \text{(C·4)}$$

Since Eq. (C·4) is same as Eq. (C·2), the velocity field $\boldsymbol{u}$ can be obtained for a given vorticity distribution ω by use of the Biot-Savart law.

From this analogy, it is clear that in Cases-A and -B in Fig. A-3 the vortices generated at the contact surface drive the fluid motion and the resultant deformation of the contact surface as shown below in Fig. A-3. It is noted that in Case-B, the generated vortices have the opposite sign against Case-A. Therefore, the vortices initially generated make the contact surface flat and overshoot to grow in the opposite direction. This is a typical property of Richitmyer-Meshkov instability. Different from the case of Rayleigh-Taylor instability, any perturbations are unstable in the case of Richitmyer-Meshkov instability.

References

1) M. D. Rosen, Phys. Plasmas **3** (1996), 1803.
2) J. M. Dawson, Phys. Fluids **7** (1964), 981.
3) See web-site of NIF; http://www.llnl.gov/nif/
4) R. Pellat, "Ignition: a dual challenge", in *IFSA99*, ed. C. Labaraune et al. (Elsevier, Paris, 2000), p. 3.
5) H. Takabe, J. Plasma Fusion Res. **69** (1993), 1285 in Japansese.
6) B. H. Ripin et al., in *Laser Interaction and Related Plasma Phenomena* (Pergamon Press, NY, 1986), vol. 7, p. 857.
7) J. Grun et al., Phys. Rev. Lett. **66** (1991), 2738; NRL Mem. Rep. 6790-94-7366 (1994).
8) B. A. Remington et al., Phys. Plasmas **4** (1997), 1994.
   P. Drake et al., Phys. Rev. Lett. **81** (1998), 2068.
   J. Kane et al., Phys. Plasmas **6** (1999), 2065.
9) B. Remington, D. Arnett, P. Drake and H. Takabe, Science **284** (1999), 1488.
10) B. Remington, R. P. Drake, H. Takabe and D. Arnett, Plasma Phys. **7** (2000), 1641.
11) B. Remington, D. Arnett, P. Drake and H. Takabe (ed.), Astrophys. J. Suppl. **127** (2000), Part 1, No. 2.
12) H. Tsunemi et al., in *Thermonuclear Supernovae*, NATO ASI Ser.(c) (Kluwer Academic Pub., Dordrecht, 1977), vol. 486, p. 561.
13) Y. Totuka, *Elementary Particle Physics* (Iwanami, Tokyo, 1992), in Japanese.
14) G. A. Mourou et al., Phys. Today **51** (1998), 22.
    C. Joshi and P. B. Corkun, Phys. Today **48** (1995), 36.
15) J. D. Lindl, *Inertial Confinement Fusion* (AIP Press and Springer, 1999).
16) M. Tabak et al., Phys. Fluids **28** (1994), 3676.
17) W. L. Kruer, *The Physics of Laser Plasma Interactions* (Addison-Wesley Pub., 1988).
18) S. I. Anisimov and V. A. Khokhlov, *Instabilities in Laser-Matter Interaction* (CRC Press, 1995).
19) Ya. B. Zel'dovich and Yu. P. Raizer, *Physics of Shock Waves and High-Temperature Hydrodynamic Phenomena* (Academic, 1966), vols. I and II, chap. X.
20) H. Takabe et al., J. Phys. Soc. Jpn. **45** (1978), 2001.
21) H. Nishimura et al., Phys. Rev. A **43** (1991), 3073.
22) R. Sigel et al., Phys. Rev. A **38** (1988), 5779.

23) H. Nishimura et al., Phys. Rev. A **44** (1991), 8323.
24) M. H. Key, in *Physics of Laser Plasmas*, Handbook of Plasma Physics, ed. A. Rubenchik and S. Witkowski (North-Holland Publ., 1991), vol. 3, p. 575.
25) H. Takabe et al., Plasma Phys. Control. Fusion **41** (1999), A75.
26) H. Azechi, private communication.
27) K. Shigemori et al., Phys. Rev. Lett. **78** (1997), 250.
28) B. Remington et al., Phys. Fluids B **5** (1995), 2589.
29) H. Azechi et al., Phys. Plasmas **4** (1997), 4079.
30) H. Shiraga et al., Rev. Sci. Instrum. **68** (1997), 745.
31) K. Fujita et al., Rev. Sci. Instrum. **72** (2001), 744.
32) C. Keane et al., J. Quant. Spectrosc. Radiat. Transfer **54** (1995), 207.
33) L. D. Landau and E. M. Lifshitz, *Fluid Mechanics* (Pergamon Press, 1959), chap. XIV.
34) R. More et al., Phys. Fluids **31** (1988), 3059.
35) R. F. Schmalz and J. Meyer-ter-Vehn, Phys. Fluids **28** (1985), 932.
36) T4-group, Los Alamos National Laboratory Report No. LALP-83-4 (1983).
37) C. Kittel, *Introduction to Solid State Physics*, 5$^{\text{th}}$ ed. (John Wiley & Sons, Inc., 1976), p. 85.
38) L. B. Da Silva et al., Phys. Rev. Lett. **78** (1997), 483.
39) S. P. Marsh (ed.), *LASL Shock Hugoniot Data* (Univ. California Press, 1980).
A. N. Mostovych et al., Phys. Plasmas **8** (2001), 2281.
40) R. Jeanloz, Phys. Today **53** (2000), 44.
G. W. Collins et al., Science **281** (1998), 1178.
41) S. T. Weir, A. C. Michell and W. J. Nellis, Phys. Rev. Lett. **76** (1996), 1860.
42) M. Ross, Phys. Rev. B **58** (1998), 669.
43) M. Koenig et al., in *Inertial Fusion Science and Applications 99* (Elsevier, 2000), p. 1127.
44) C. C. Petersen and J. C. Brandt, *Hubble Vision*, 2nd ed. (Cambridge Univ. Press, 1998), p. 6.
45) X. Yang et al., Phys. Fluids A **4** (1992), 1531.
46) H. Takabe, "Inertial Confinement Fusion and Hydrodynamic Instabilities (1), (2), (3)", J. Plasma Fusion Res. **73** (1997), 147, 313, 395 in Japanese.
47) N. Cowpwerthwaite, Physica D **37** (1989), 264.
48) N. Cowpwerthwaite et al., in *Compressible Turbulent Mixing*, ed. R. Young et al. (World Scientific, 1996), p. 147.
49) N. Zabusky et al., Phys. Today **46** (1993), 22.
50) A. Sunahara et al., Jpn. J. Appl. Phys. **35** (1996), 5501.
51) J. M. Stone and M. L. Norman, Astrophys. J. **390** (1992), L17.
52) R. I. Klein et al., Astrophys. J. Suppl. **127** (2000), 379.
53) M. M. Marinak, Phys. Plasmas **8** (2001), 2275.
54) See web-site of ASCI project, http://www.llnl.gov/asci/
55) See web-site, http://oposite.edu/pubinfo/PR/2000/11/pr.html
56) See Chandra web-site; http://chandra.harvard.edu/00_releases/press_051100sn1987a.html
57) H. Takabe et al., in *Numerical Astrophysics* (Kluwer Acad. Publ., London, 1999), p. 423.
Y.-G. Kang et al., in *Inertial Fusion Science and Applications 99* (Elsevier, 2000), p. 1061.
58) H. Takabe et al., Plasma Phys. Control. Fusion **41** (1999), A75.
59) H. Takabe et al., Phys. Fluids **31** (1988), 2884.
60) F. Hattori et al., Phys. Fluids **29** (1986), 1719.
61) For example, W. D. Arnnet et al., Annu. Rev. Astron. Astrophys. **27** (1989), 627.
W. Hillebrandt and P. Hoflich, Rep. Prog. Phys. **52** (1989), 1421.
I. Hachisu et al., Astrophys. J. **390** (1992), 230.
62) S. Kumagai et al., Astrophys. J. **345** (1989), 412.
63) T. Shigeyama, Publ. Astron. Soc. Jpn. **47** (1998), 581.
64) H. Takabe and T. Ishii, Jpn. J. Appl. Phys. **32** (1993), 5675.
65) T. Ebisuzaki et al., Astrophys. J. **344** (1989), L65.
66) K. Budil, private communication.
67) E. Muller et al., Astron. Astrophys. **251** (1991), 505.
68) R. A. Chevalier et al., Astrophys. J. **392** (1992), 118.
69) R. A. Chevalier et al., Astrophys. J. **444** (1995), 312.
70) For example, B. Schwarzschild, Phys. Today **52** (1999), 19.

71) C. J. Hogan et al., Scientific American, January (1999), 28.
72) F. A. Williams, *Combustion Theory*, 2nd ed. (Benjamin Pub., 1984), chap. 9.5.
73) F. X. Timmes, Astrophys. J. **423** (1994), L131.
74) K. Nomoto et al., Astrophys. J. **284** (1984), 644.
75) S. I. Blinnikov and P. V. Sasorov, Phys. Rev. E **53** (1996), 4827.
76) W. Hillebrandt and J. Niemeyer, Ann. Rev. Astron. Astrophys. **38** (2000), 191.
77) D. Shvarts et al., Phys. Plasmas **2** (1995), 2465.
D. Oron et al., Phys. Plasmas **8** (2001), 2883.
78) See web-site, http://oposite.stsci.edu/pubinfo/pr/1998/18/greatest-hits-gallery.html
79) L. Spitzer Jr., Astrophys. J. **120** (1954), 1.
80) C. Verdon et al., Phys. Fluids **25** (1982), 1653.
81) R. G. Evans et al., Phys. Rev. Lett. **49** (1982), 1639.
82) M. W. Pound et al., Astrophys. J. **493** (1998), L113.
83) J. Kane, private communication.
84) H. Takabe et al., Phys. Fluids **28** (1985), 3676.
85) K. S. Budil et al., Phys. Rev. Lett. **76** (1996), 4536; Phys. Plasmas **8** (2001), 2344.
86) F. J. D. Serduke et al., J. Quantum Spectrosco. Radiat. Transfer **65** (2000), 527.
87) W. Dappen, in *Elementary Processes in Dense Plasmas*, ed. S. Ichimaru and S. Ogata (Addison-Wesley Pub., 1995), p. 203.
88) F. J. Rogers and C. A. Iglesias, Science **263** (1994), 50.
89) T. S. Perry et al., Phys. Rev. E **54** (1996), 5617.
90) M. Kato and I. Hachisu, Astrophys. J. **437** (1994), 802.
91) C. C. Petersen and J. C. Brandt, *Hubble Vision*, 2nd ed. (Cambridge Univ. Press, 1998), p. 93.
92) P. Moskalik et al., Astrophys. J. **385** (1992), 685.
93) F. J. Rogers and C. A. Iglesias, in *Elementary Processes in Dense Plasmas*, ed. S. Ichimaru and S. Ogata (Addison-Wesley Pub., 1995), p. 181.
94) For example, F. H. Shu, *The Physics of Astrophysics (1) "Gas Dynamics"* (University Science Press, 1992), chap. 17.
95) For example, J. Meyer-ter-Vehn, Z. Naturforsch **37a** (1982), 955.
96) R. E. Kidder, Nucl. Fusion **16** (1976), 3.
97) F. Hattori et al., Phys. Fluids **29** (1986), 1719.
98) Ya. B. Zel'dovich and Yu. P. Raizer, *Physics of Shock Waves and High Temperature Hydrodynamic Phenomena* (Academic Press, New York, 1966), chaps. X & XII.
99) Page 611 in chapter IX of Ref. 98), vol. II.
100) K. Koyama, private communications.
101) E. M. Eppeline, Laser Particle Beams **12** (1994), 257.
102) T. E. Giover et al., Phys. Rev. Lett. **75** (1995), 445.
103) T. Kato, Physica Scripta **T73** (1997), 98.
104) See web-site of Yohkoh, http://isass1.solar.isas.ac.jp/
105) Detail is given in; T. Tajima and K. Shibata, *Plasma Astrophysics* (Addison Wesley, 1997), p. 243.
106) E. T. Vishniac, Astrophys. J. **274** (1983), 152.
E. T. Vishniac and D. Ryu, Astrophys. J. **337** (1989), 917.
M. M. Mac Low and M. L. Norman, Astrophys. J. **407** (1993), 207.
107) Page 98 in Ref. 98), vol. I.
108) D. T. Haar (ed.), *Collected Paper of L. D. Landau* (Pergamon Press, 1965), p. 396. Problem 1 at p. 478 in chap. XIV of Ref. 33).
109) J. M. Blondin et al., Astrophys. J. **500** (1998), 342.
110) D. A. Tidman and N. A. Krall, *Shock Waves in Collisionless Plasmas* (Wiley-Interscience, 1971).
111) P. Drake, Phys. Plasmas **7** (2000), 4690.
112) B. H. Ripin et al., Phys. Fluids **B5** (1993), 3491.
113) V. M. Antonov et al., in *Laser Interaction with Matter*, ed. S. Rose, IOP Conf. Ser. No. 140 (IOP, 1995), p. 167.
114) For example, p. 80 in Ref. 91).
115) R. S. Furuya et al., Astrophys. J. **525** (1999), 821; **542** (2000), L135.
116) J. M. Blondin et al., Astrophys. J. **360** (1990), 370.

117) J. M. Stone and M. L. Norman, Astrophys. J. **413** (1993), 198.
118) A. Mizuta, S. Yamada and H. Takabe, "Numerical Analysis of Jets Produced by Intense Lasers", submitted to Astrophys. J. (2001).
119) D. R. Farley et al., Phys. Rev. Lett. **83** (1999), 1982.
120) K. Shigemori et al., Phys. Rev. E **62** (2000), 8838.
121) For example, C. H. Townes, *How the Laser Happened* (Oxford Univ. Press, New York, 1999), chap. 9.
122) P. J. Benson et al., Astrophys. J. Suppl. **74f** (1990), 911.
123) M. Miyoshi et al., Nature **371** (1994), 395.
124) K. Kawashima and S. Kitamoto, Publ. Astron. Soc. Jpn. **48** (1996), L113.
125) For example, F. H. Shu, *The Physical Universe, An Introduction to Astronomy* (University Science Books, 1982), p. 198.
126) F. Parerels et al., Astrophys. J. **533** (2000), L135.
127) B. Tarter et al., Astrophys. J. **156** (1969), 943.
128) T. R. Kallman and R. McCray, Astrophys. J. Suppl. **50** (1982), 263.
129) Y. Morita et al., J. Quant. Spectrosc. Radit. Transfer, to be published (2001).
130) H. Takabe and Y. Morita, "Possibility of X-Ray Lasers in Universe", J. Plasma Fusion Res. **77** (2001), 441 in Japanese.
131) M. Perry et al., Science & Technology Review (Lawrence Livermore National Laboratory, December 1996), p. 4; Science & Technology Review (Lawrence Livermore National Laboratory, March 2000), p. 4
132) Y. Kitagawa et al., *Petawatt Laser for Fast Ignitor and Laser Matter Interaction Researches*, CLEO/Pacific Rim 2001, MC2-1 (4th Pacific Rim Conference on Lasers and Electro-Optics, Makuhari Messe, Chiba, 15–19 July, 2001).
133) K. Yamakawa et al., Opt. Lett. **23** (1998), 1468.
134) K. Yamakawa et al., Report of Kansai Research Establishment 1999, JAERI-Review 2001-003, pp.7–9 (March 2001).
135) J. Dawson, Phys. Plasmas **6** (1999), 4436.
See also K. Nakajima, Laser Particle Beams **18** (2000), 519.
136) D. Gordon et al., Phys. Rev. Lett. **80** (1998), 2133.
137) T. E. Cowan et al., Phys. Rev. Lett. **84** (2000), 903.
138) T. E. Cowan, *Nuclear Fission and Anti-Matter Creation with Ultra Intense Laser at LLNL* (Press release at APS meeting, Atlanta, March 2000).
139) K. Nakashima and H. Takabe, "Numerical Study of Positron Energy Spectrum Produced by Ultra-Intense Lasers", submitted to Phys. Plasmas (2001).
140) J. W. Shearer et al., Phys. Rev. A **8** (1973), 1582.
141) E. P. Liang et al., Phys. Rev. Lett. **81** (1998), 4887.
142) D. A. Gryaznkh et al., JETP Lett. **67** (1998), 257.
143) T. Tamae, private communication.
P. Durapal and D. S. Onley, Phys. Rev. C **27** (1983), 523.
144) T. E. Cowan et al., Laser Particle Beams **17** (1999), 773;
See also C. Gahn et al., Appl. Phys. Lett. **77** (2000), 2662.
145) L. D. Landau and E. M. Lifshitz, *Statistical Physics*, 3rd ed. (Pergamon, New York, 1976), sec. 105.
146) R. Svenssen, Astrophys. J. **258** (1982), 335, Fig. 8.
147) C. Hayashi and S. Hayakawa, *Astrophysics* (Iwanami, Tokyo, 1978), p. 98 in Japanese.
148) S. L. Shapiro and S. A. Teukolsky, *Black Holes, White Dwarfs, and Neutron Stars* (Wiley Int. Pub., New York, 1983), chap. 10.
149) F. Takahara, J. Plasma Fusion Res. **74** (1998), 1305 in Japanese.
150) L. Bouchet et al., Astrophys. J. **383** (1991), L45.
151) M. Leventhal et al., Astrophys. J. **225** (1978), L11.
152) J. Fukue, Parity **8** (1993), 50 in Japanese.
153) B. Margon, Ann. Rev. Astron. Astrophys. **22** (1984), 507.
154) T. Kotani, J. Plasma Fusion Res. **76** (2000), 642 in Japanese.
155) N. Nakai et al., Nature **361** (1993), 45.
156) J. R. Herrnstein et al., Nature **400** (1999), 539.
157) C. L. Carilli et al., Phys. Plasmas **5** (1998), 1981.
158) A. S. Wilson et al., astro-ph/0009308 (19 Sep 2000).

159) H. Hirabayashi, BUTSURI **56** (2001), 308 in Japanese.
160) J. F. Wardle et al., Nature **395** (1999), 457.
161) K. Hirotani et al., Publ. Astron. Soc. Jpn. **51** (1999), 263.
162) S. Kamano and K. Hirotani, J. Plasma Fusion Res. **76** (2000), 648 in Japanese.
163) S. M. Mahajan et al., Phys. Plasmas **5** (1998), 3264.
164) T. Galama, Astronomy & Geology (A & G) **40** (1999), 5.10.
165) M. R. Metzger et al., Nature **387** (1997), 878.
166) S. Blinnikov, private communication.
167) P. Meszaros and M. Ress, Astrophys. J. **405** (1993), 278.
168) T. Piran, Phys. Rep. **314** (1999), 575.
169) K. Iwamoto et al., Nature **395** (1998), 672.
E. Baron, Nature **395** (1998), 635.
170) A. I. MacFadyen and S. E. Woosley, Astrophys. J. **524** (1999), 262.
171) A. Pukov and J. Meyer-ter-Vehn, Laser Particle Beams **17** (1999), 571.
172) S. C. Wilks et al., Phys. Rev. Lett. **69** (1992), 1383.
173) A. Pukov and J. Meyer-ter-Vehn, Phys. Rev. Lett. **79** (1997), 2686.
174) A. Pukov and J. Meyer-ter-Vehn, Phys. Plasmas **5** (1998), 1880.
175) S. Hatchett et al., Phys. Plasmas **7** (2000), 2076.
176) S. C. Wilks et al., Phys. Plasmas **8** (2001), 542.
177) M. Roth, private communications (2001).
178) H. Ruhl, private communications (2001).
179) G. Mourou, private communications (2000).
180) S. Karch et al., Laser Particle Beams **17** (1999), 565.
181) See GEANT web-site, http://wwwinfo.cern.ch/asd/geant/
182) H. Takabe (ed.), the special issue on *Laser Nuclear Physics*, J. Plasma Fusion Res., to be published in November issue in English (2001).
183) L. D. Landau and E. M. Lifshitz, *The Classical Theory of Fields*, 4th ed. (Pergamon Press, Oxford, 1975), chap. 10.
184) T. Ebisuzaki, private communications.
185) G. Schafer and R. Sauerbrey, "Probing Black-Hole Physics in the Laboratory Using Intense Femtosecond Lasers", astro-ph/9805106 (8 May, 1998).
186) H. Takabe, in *Exploding Phenomena in Astrophysical Compact Objects*, ed. H. Y. Chang et al. (AIP Conf. Proc. vol. 556, 2001), p. 398.
187) H. Yukawa, "*Tabibito (The Traveler)*" (World Scientific Publ., 1982).
188) A. Pukov and J. Meyer-ter-Vehn, Phys. Rev. Lett. **76** (1996), 3975.
189) O. L. Larden et al., ICF Quarterly Report (LLNL) **15** (1995), 271.
190) G. Jordan and H. Houas (ed.), *The Physics of Compressible Turbulent Mixing* (Marseille, Impremerie Caractere, 1997).
191) J. Bauche et al., Phys. Rev. A **20** (1979), 2424.
192) A. Bar-Shalom et al., Phys. Rev. A **40** (1989), 3183.
193) M. Klapisch et al., Phys. Plasmas **8** (2001), 1817.
194) A. N. Langdon, Phys. Rev. Lett. **44** (1980), 575.
195) J. Albritton, Phys. Rev. Lett. **50** (1983), 2078.
196) L. Spitzer and R. Harm, Phys. Rev. **89** (1953), 977.
197) S. I. Braginskii, *Review of Plasma Physics* (Consultant Bureau, NY, 1965), vol. 1, p. 205.
198) A. R. Bell et al., Phys. Rev. Lett. **46** (1981), 243.
199) C. Yamanaka, in Ref. 24), p. 26.
200) J. F. Luciani et al., Phys. Rev. Lett. **51** (1983), 1664.
201) A. Nishiguchi et al., Phys. Fluids B **4** (1992), 417.
202) A. Sunahara, private communications.
203) J. R. Davies et al., Phys. Rev. E **56** (1997), 7193.